

THE SURFACE-TENSION-DRIVEN RETRACTION OF A VISCIDA*

I. M. GRIFFITHS[†] AND P. D. HOWELL[†]

Abstract. We consider the surface-tension-driven evolution of a thin two-dimensional sheet of viscous fluid whose ends are held a fixed distance apart. We find that the evolution is governed by a nonlocal nonlinear partial differential equation, which may be transformed, via a suitable change of time variable, to a simple linear equation. This possesses an interesting dispersion relation which indicates that it is well posed whether solved forwards or backwards in time, enabling us to determine which initial shapes will evolve to a given shape at a later time. We demonstrate that our model may be used to describe the global evolution of a viscida containing small regions of high curvature, and proceed to investigate the evolution of a profile which contains a corner. We show that the corner is not smoothed out but persists for forward and inverse time. The introduction of a pressure differential across the free surfaces is shown to provide a method of controlling the shape evolution.

Key words. thin-film flows, asymptotic analysis, incompressible viscous fluids

AMS subject classifications. 76D99, 35G10

DOI. 10.1137/090746318

1. Introduction. In this paper we study the evolution of a viscous fluid occupying a two-dimensional domain whose inverse aspect ratio ϵ is small so that it may be described as a thin viscous sheet or *viscida* [1, 2]. In addition, we suppose that the dimensionless curvature is of the same order as ϵ so that the viscida is almost flat. We examine how such a viscida evolves either under the action of surface tension alone or with an applied pressure difference, while the ends are simply held in position. The small parameter ϵ is exploited through a systematic asymptotic analysis of the problem.

There have been many investigations into the evolution of two-dimensional viscous sheets. In particular, Buckmaster, Nachman, and Ting [1] consider the buckling of a viscida when the ends are moved towards each other. The cases where the sheet curvature is small and order one are both considered, and the effects of surface tension are included in [2]. Many of the results of the perturbative analysis followed in this paper are also obtained in [1] and [2]. However, here we follow a more systematic approach based on asymptotic analysis of the governing Stokes equations and boundary conditions, without using any ad hoc kinematic assumptions. At the same time, we incorporate an applied pressure drop across the viscida.

The relevance of the stretching of a thin viscida to the drawing of glass sheets is investigated in [11], and comparisons may be made between those results and ours concerning the evolution of a viscida with clamped ends. Van de Fliert, Howell, and Ockendon [3] examine the stretching of a two-dimensional viscida under an applied pressure, motivated by the formation of bottles by glass blowing, while the influence of gravity is addressed in [10].

There are two distinct timescales over which a viscous sheet evolves [6]: a short *bending* timescale on which the center-line relaxes to a straight line, while the thickness

*Received by the editors January 12, 2009; accepted for publication (in revised form) August 25, 2009; published electronically December 11, 2009. This research was supported by a studentship from the University of Oxford's EPSRC-funded doctoral training account.

<http://www.siam.org/journals/siap/70-5/74631.html>

[†]Mathematical Institute, University of Oxford, 24-29 St. Giles', Oxford, OX1 3LB, UK (ian.griffiths@maths.ox.ac.uk, howell@maths.ox.ac.uk).

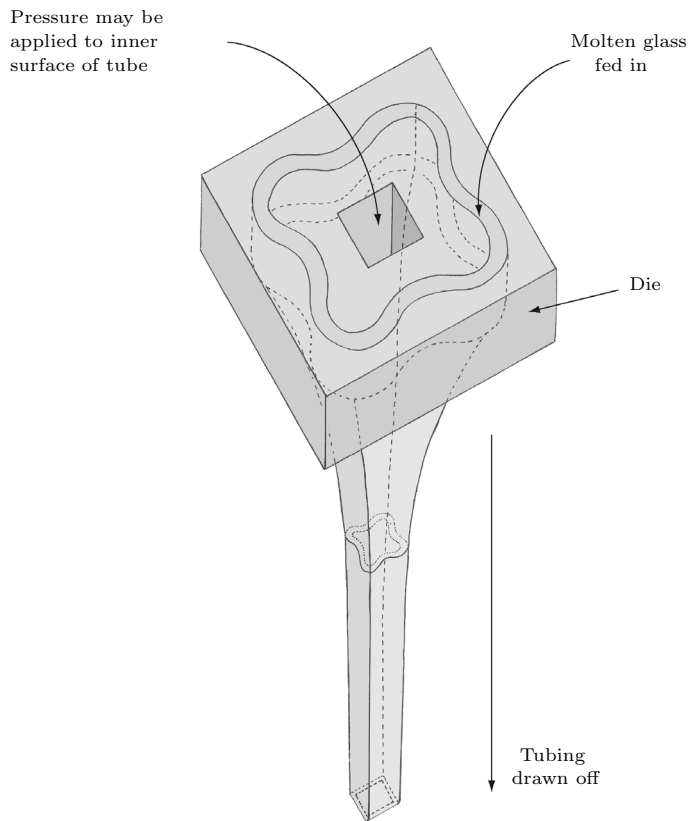


FIG. 1.1. Schematic diagram of the Vello process for the construction of square capillary tubing.

remains unchanged; and a longer *stretching* timescale over which the thickness evolves. When a pressure differential is applied, there are similarly two distinguished limits. A sufficiently high applied pressure will cause a viscida to form a circular arc and then undergo viscous stretching. In this paper we are concerned with the short-timescale low-pressure regime in which the applied pressure affects only the bending. A uniformly valid theory which incorporates the effects of an applied pressure on both the stretching and bending of a viscida is considered by Ribe [7].

Our study is motivated by the fabrication of glass tubing with a square or rectangular cross-sectional profile. In a typical process, molten glass is fed through a die and the cross-section evolves under the action of surface tension and internal pressurization to produce the desired final tube profile as illustrated in Figure 1.1. The resulting tubing has many applications, for example, as bottles in the medical industry and for square optical fibers [12, 13].

It has been shown in [5] that the evolution of the tube cross-section with axial position may be described by the time evolution of a two-dimensional closed viscida when expressed in a suitably Lagrangian scaled coordinate system. The two-dimensional evolution of such a viscida is considered in [4]. Here we consider a prototype problem, namely, the evolution of a viscida whose ends are held a fixed distance apart. This allows us to draw conclusions on how we might expect a corner region to evolve in the tube-drawing process and sheds light on the crucial inverse problem of determining the initial shape required to evolve into some desired final configuration.

We begin in section 2 by stating the governing equations. By integrating across the viscida, we obtain three global equations representing net force and torque balances. Closure relations for these are obtained in section 3 by nondimensionalizing the equations and taking an asymptotic limit as ϵ tends to zero. We thus obtain an evolution equation for the center-line of the viscida. We find that the introduction of a new time variable allows us to write down the solution explicitly and recover the real time variable a posteriori via an algebraic relation.

We are particularly interested in the evolution of a viscida containing a corner. To validate our model in such a regime, we first consider a profile with a small region of high, but finite, curvature. We increase the curvature so that the profile approaches a corner configuration and find that this does not generate any adverse effects on the global profile evolution. We infer that our small-curvature model may be used to describe the global evolution of a viscida containing isolated regions of high curvature. The local motion near such a corner is described by the full two-dimensional Stokes equations but does not influence the global sheet evolution in which we are interested.

A fortuitous consequence of our asymptotic limit is the elimination of high-wavenumber disturbances so that the problem is well posed for both forward and inverse time. This allows us to determine the profile which would generate a corner in the viscida at a later time. A further surprising result is that, on the timescale of interest, an initial corner persists both for forward and inverse time and is not smoothed out as we might have anticipated.

We then investigate the effect of applying a pressure differential across the viscida in section 5. This removes the existence of a simple analytic solution, but the equations are easily solved using a numerical time-stepping scheme. We find that many of the important features are retained, in particular the well posedness for inverse time and the persistence of corners, but that the inclusion of such a pressure difference allows for additional control on the viscida evolution.

In section 6, we examine the linear stability of a viscida of small but finite thickness. This demonstrates that the full two-dimensional Stokes flow model is ill posed as an inverse problem, and explains how it is regularized by taking our thin-film limit. Finally, in section 7, we discuss the implications of our results and draw analogies between the paradigm problem considered here and the manufacture of polygonal glass tubing.

2. Governing equations and boundary conditions. We use a Cartesian coordinate system (x, y) , denoting the position of the center-line at time t by $y = H(x, t)$ and the thickness of the sheet by $h(x, t)$, so that the upper and lower surfaces lie at $y = H \pm h/2$, respectively. We consider a sheet which lies in the range $0 \leq x \leq \mathcal{L} = \text{constant}$, so the center-line length is given by

$$(2.1) \quad L(t) = \int_0^{\mathcal{L}} \sqrt{1 + H_x^2} \, dx.$$

The curvatures of the center-line $\kappa(x, t)$ and of the upper and lower surfaces $\kappa^\pm(x, t)$ are given by

$$(2.2) \quad \kappa = \frac{H_{xx}}{(1 + H_x^2)^{3/2}}, \quad \kappa^\pm = \frac{(H_{xx} \pm \frac{1}{2}h_{xx})}{(1 + (H_x \pm \frac{1}{2}h_x)^2)^{3/2}}.$$

We neglect inertia and body forces so that the governing equations for the fluid

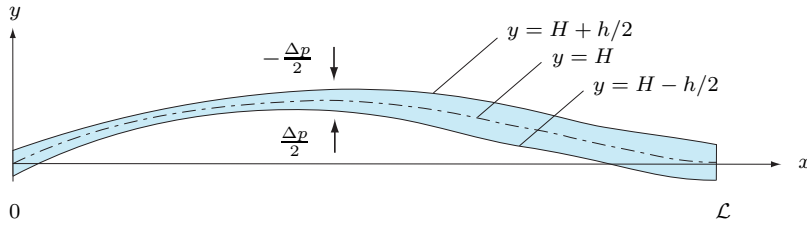


FIG. 2.1. Definition sketch of the model problem.

evolution are the Stokes equations

$$(2.3) \quad \frac{\partial u}{\partial x} + \frac{\partial v}{\partial y} = 0,$$

$$(2.4) \quad \frac{\partial \sigma_{xx}}{\partial x} + \frac{\partial \sigma_{xy}}{\partial y} = 0,$$

$$(2.5) \quad \frac{\partial \sigma_{xy}}{\partial x} + \frac{\partial \sigma_{yy}}{\partial y} = 0,$$

where $\mathbf{u} = (u, v)$ denotes the fluid velocity. For an incompressible Newtonian fluid, the stress components are given by

$$(2.6) \quad \sigma_{ij} = -p\delta_{ij} + \mu \left(\frac{\partial u_i}{\partial x_j} + \frac{\partial u_j}{\partial x_i} \right),$$

where p represents the fluid pressure and μ is the dynamic viscosity, which we assume to be constant.

The kinematic and dynamic boundary conditions on the surfaces of the viscida are, respectively,

$$(2.7) \quad v = H_t \pm h_t/2 + u(H_x \pm h_x/2),$$

$$(2.8) \quad \sigma_{xy} = \sigma_{xx}(H_x \pm h_x/2) \mp (H_x \pm h_x/2)\gamma\kappa^\pm \mp (H_x \pm h_x/2)\Delta p/2,$$

$$(2.9) \quad \sigma_{yy} = \sigma_{xy}(H_x \pm h_x/2) \pm \gamma\kappa^\pm \pm \Delta p/2$$

on $y = H \pm h/2$, where γ is the coefficient of surface tension and Δp is the pressure difference across the sheet, which we assume to be spatially uniform. A positive value of Δp represents pressurization from below. The problem is closed by specifying the initial shape of the viscida and boundary conditions at each end, for example, simply-supporting the ends or clamping them at constant angles. A schematic diagram of the set-up is shown in Figure 2.1.

It is advantageous to use the following: global force balances in the x - and y -directions, obtained by integration of (2.4) and (2.5) over the thickness of the sheet and use of (2.8) and (2.9); and a global torque balance obtained by multiplying (2.4) by y before integrating across the sheet. The resulting equations may be written as

$$(2.10) \quad \mathcal{A}_x = \Delta p H_x,$$

$$(2.11) \quad \mathcal{B}_x = -\Delta p,$$

$$(2.12) \quad \mathcal{M}_x = \mathcal{B} - \mathcal{A}H_x + \frac{1}{4}hh_x\Delta p,$$

where

$$(2.13) \quad \mathcal{A} = \int_{H-\frac{1}{2}h}^{H+\frac{1}{2}h} \sigma_{xx} \, dy + \frac{\gamma}{\sqrt{1 + (H_x + \frac{1}{2}h_x)^2}} + \frac{\gamma}{\sqrt{1 + (H_x - \frac{1}{2}h_x)^2}},$$

$$(2.14) \quad \mathcal{B} = \int_{H-\frac{1}{2}h}^{H+\frac{1}{2}h} \sigma_{xy} \, dy + \frac{\gamma(H_x + \frac{1}{2}h_x)}{\sqrt{1 + (H_x + \frac{1}{2}h_x)^2}} + \frac{\gamma(H_x - \frac{1}{2}h_x)}{\sqrt{1 + (H_x - \frac{1}{2}h_x)^2}},$$

$$(2.15) \quad \mathcal{M} = \int_{H-\frac{1}{2}h}^{H+\frac{1}{2}h} (y - H)\sigma_{xx} \, dy + \frac{\gamma h(H_x + \frac{1}{2}h_x)}{2\sqrt{1 + (H_x + \frac{1}{2}h_x)^2}} + \frac{\gamma h(H_x - \frac{1}{2}h_x)}{2\sqrt{1 + (H_x - \frac{1}{2}h_x)^2}},$$

which represent, respectively, the total tension, shear, and bending moment in the viscida, due to both viscous and surface tension effects.

We emphasize that no approximations have been employed thus far and hence (2.10)–(2.12) are exact for two-dimensional Stokes flow. However, they are underdetermined, and it remains to derive an evolution equation for the viscida thickness h and a constitutive relation for the bending moment \mathcal{M} . This will be done in the following section by nondimensionalizing the equations and exploiting the smallness of the inverse aspect ratio ϵ .

3. Perturbative analysis.

3.1. Nondimensionalization. We suppose that the curvatures are of order ϵ/\mathcal{L} , while the timescale for center-line motion is fixed by a balance between surface tension and viscosity. The y -velocity scale is fixed by the kinematic boundary condition to provide nonzero leading-order sheet motion. Thus we set

$$(3.1) \quad \begin{aligned} (x, y) &= \mathcal{L}(x', \epsilon y'), & t &= \frac{\epsilon^3 \mu \mathcal{L}}{\gamma} t', & (u, v) &= \frac{\gamma}{\epsilon^2 \mu} (\epsilon u', v'), & p &= \frac{\gamma}{\epsilon \mathcal{L}} p', \\ H &= \epsilon \mathcal{L} H', & h &= \epsilon \mathcal{L} h', & \kappa &= \frac{\epsilon}{\mathcal{L}} \kappa', & \kappa^\pm &= \frac{\epsilon}{\mathcal{L}} \kappa^{\pm'}, & L &= \mathcal{L} L', \end{aligned}$$

while the components of the stress tensor and total tensions and bending moment are nondimensionalized via

$$(3.2) \quad \sigma_{xx} = \frac{\gamma}{\epsilon \mathcal{L}} \sigma'_{xx}, \quad \sigma_{xy} = \frac{\gamma}{\mathcal{L}} \sigma'_{xy}, \quad \sigma_{yy} = \frac{\epsilon \gamma}{\mathcal{L}} \sigma'_{yy},$$

$$(3.3) \quad \mathcal{A} = \gamma \mathcal{A}', \quad \mathcal{B} = \frac{\gamma}{\epsilon} \mathcal{B}', \quad \mathcal{M} = \epsilon \gamma \mathcal{L} \mathcal{M}',$$

where the scalings have been chosen to ensure that all terms are nonzero at leading order. For a molten glass viscida held a distance $\mathcal{L} = 10$ cm apart with an inverse aspect ratio of $\epsilon = 0.1$, viscosity $\mu = 10^6$ N s⁻¹, and $\gamma = 0.3$ N m⁻¹, a typical timescale of evolution is of the order of 10² s.

3.2. Distinguished limit. Before we can pose asymptotic expansions for the dependent variables, we have to decide how to scale the applied pressure, and it transpires that there are two distinguished limits. Here we will assume that the dimensionless pressure drop

$$(3.4) \quad P = \frac{\Delta p \mathcal{L}}{\epsilon \gamma}$$

is an order-one parameter. With this choice, changes in the shape of the viscida are influenced by both applied pressure and surface tension, but we will find that the pressure then has no effect on the thickness of the viscida. Choosing the applied pressure to be larger by a factor of $O(1/\epsilon^2)$ induces stretching of the viscida but forces it instantaneously to form a circular arc. Such a scenario is considered in the order-one-curvature regime in [3]. A model which incorporates an applied pressure that affects both stretching and bending in a viscida is considered in [7].

Having chosen the appropriate scaling for the applied pressure, we now expand all dependent variables as regular parameter expansions of the form $H' = H^{(0)} + \epsilon^2 H^{(1)} + \epsilon^4 H^{(2)} + \dots$. Below we just present the resulting leading-order equations, dropping the superscript (0) for clarity of notation.

3.3. Leading-order analysis. The global force and torque balances (2.10)–(2.12) at leading order imply that

$$(3.5) \quad \mathcal{M}_{xx} = -P - \mathcal{A}H_{xx},$$

where $\mathcal{A} = \mathcal{A}(t)$. Equation (3.5) is the generalization of the governing equation obtained in [1] to account for an applied pressure. We adopt a similar approach to [1] and use our systematic perturbative analysis to produce functional relations for both \mathcal{M} and \mathcal{A} in terms of H so that (3.5) becomes the evolution equation for the center-line of the sheet.

Leading-order analysis of the governing equations (2.3)–(2.5) and boundary conditions (2.7)–(2.9) gives

$$(3.6) \quad h_t = 0,$$

$$(3.7) \quad v = H_t,$$

$$(3.8) \quad u = \mathbf{u} + H_{xt}(H - y),$$

where

$$(3.9) \quad \mathbf{u} = \mathbf{u}(x, t) = \frac{1}{h} \int_{H-h/2}^{H+h/2} u(x, y, t) dy$$

is the average leading-order horizontal sheet velocity. Equation (3.6) informs us that the thickness of the viscida is conserved on this timescale. In addition, as expected by mass conservation, the leading-order sheet length $L = 1$ by (2.1). Equation (3.8) indicates that the fluid velocity is a linear function of y . The \mathbf{u} and $H_{xt}(H - y)$ terms correspond to extensional and bending components, respectively. Thus in this asymptotic model both stretching and bending effects are important in the sheet evolution.

Analysis of the governing equations at second order in ϵ provides leading-order expressions for the tension and bending moment, namely,

$$(3.10) \quad \mathcal{A} = 4(\mathbf{u}_x + H_x H_{xt})h + 2,$$

$$(3.11) \quad \mathcal{M} = -\frac{1}{3}H_{xxt}h^3.$$

The bracketed term in the leading-order tension (3.10) represents the contribution due to viscous stretching, while the surface tension appears as the final (constant) term. The bending moment (3.11), however, is unchanged from [2], indicating that, to leading order, surface tension manifests itself only in the total tension, and does not affect the bending moment.

3.4. A uniformly thick viscida. Henceforth we consider a viscida whose thickness is initially uniform. Then (3.6) implies that h is constant for all t , and if we define ϵ specifically as the ratio of initial sheet thickness to length, then $h(x, t) \equiv 1$. We fix $u(0, t) = 0$, eliminating rigid-body translations in the x -direction, and $u(1, t) = 0$ since the viscida is fixed at $x = 1$. Integration of (3.10) then gives

$$(3.12) \quad \mathcal{A} = 2 \frac{d}{dt} \int_0^1 H_x^2 dx + 2 = 4 \frac{dL^{(1)}}{dt} + 2,$$

where $dL^{(1)}/dt$ is the lowest-order rate of change of sheet length (recalling that $L^{(0)} \equiv 1$), and represents the viscous contribution to the total tension in the sheet. Substituting for the leading-order bending moment (3.11) in (3.5) gives

$$(3.13) \quad \frac{1}{3} H_{xxxxt} = \mathcal{A} H_{xx} + P.$$

Equations (3.12) and (3.13) form a set of coupled equations for \mathcal{A} and H , which may be combined to give the nonlinear, nonlocal evolution equation

$$(3.14) \quad \frac{1}{3} H_{xxxxt} = 2 \left[\frac{d}{dt} \int_0^1 H_x^2 dx + 1 \right] H_{xx} + P$$

for the center-line of the sheet. When $P < 0$, (3.13) also describes the sagging of a small-curvature viscida under the influence of gravity [10].

This system requires four boundary conditions and one initial condition. We assume that the ends are held at fixed positions so that

$$(3.15) \quad H(0, t) = H(1, t) = 0.$$

The final two boundary conditions may be zero bending moment, or *simple support*, that is,

$$(3.16) \quad H_{xxt}(0, t) = H_{xxt}(1, t) = 0;$$

clamped ends at constant angle

$$(3.17) \quad H_{xt}(0, t) = H_{xt}(1, t) = 0;$$

or some combination of the above.

4. Zero applied pressure.

4.1. Problem transformation. We apply the change of variable

$$(4.1) \quad \tau = 3 \int_0^t \mathcal{A}(t') dt',$$

which, after use of (3.12), gives

$$(4.2) \quad t = \frac{1}{6} \tau - \int_0^1 H_x(x, \tau)^2 - H_x(x, 0)^2 dx.$$

When $P = 0$, (3.13) is then transformed to

$$(4.3) \quad H_{xxxx\tau} = H_{xx}.$$

Since

$$(4.4) \quad \frac{dt}{d\tau} = \frac{1}{6} + 2 \int_0^1 H_{xx\tau}^2 dx - 2[H_{x\tau}H_{xx\tau}]_0^1 > 0$$

for profiles that are either simply supported or clamped, (4.1) defines a one-to-one relationship between τ and t .

As we will shortly demonstrate, (4.3) is readily solved, for example, by separation of variables, and the tension is obtained from (3.12) in the form

$$(4.5) \quad \mathcal{A}(\tau) = \frac{2}{1 - 6 \frac{d}{d\tau} \int_0^1 H_x(x, \tau)^2 dx},$$

while (3.12) and (4.1) provide the sheet length

$$(4.6) \quad L^{(1)}(t) = L^{(1)}(0) + \frac{\tau}{12} - \frac{t}{2}.$$

Equation (4.2) is then used to recover the physical time and complete the solution.

4.2. A simply supported viscida. To begin with, we will consider the case where the ends of the viscida are simply-supported. Integrating (4.3) and applying the conditions (3.15) and (3.16) gives the equation

$$(4.7) \quad H_{xx\tau} = H.$$

This has solution

$$(4.8) \quad H = \int_0^1 H_{\zeta\zeta}(\zeta, 0)G(x, \zeta, \tau) d\zeta,$$

where

$$(4.9) \quad G(x, \zeta, \tau) = -\frac{2}{\pi^2} \sum_{n=1}^{\infty} \frac{\sin(n\pi x) \sin(n\pi\zeta)}{n^2} e^{-\tau/n^2\pi^2}$$

is a Green's function, defined to satisfy

$$(4.10a) \quad \frac{\partial^3 G}{\partial x^2 \partial \tau} = G, \quad 0 < x < 1, \quad \tau > 0,$$

$$(4.10b) \quad G = 0, \quad x = 0, 1, \quad \tau > 0,$$

$$(4.10c) \quad G = -x(1 - \zeta), \quad 0 < x < \zeta, \quad \tau = 0,$$

$$(4.10d) \quad G = -\zeta(1 - x), \quad \zeta < x < 1, \quad \tau = 0.$$

The relation between τ and t is then given by (4.2) as

$$(4.11) \quad t = \frac{\tau}{6} + \sum_{n=1}^{\infty} \frac{2}{n^2\pi^2} \left(\int_0^1 H_{\zeta\zeta}(\zeta, 0) \sin(n\pi\zeta) d\zeta \right)^2 \left(1 - e^{-2\tau/n^2\pi^2} \right),$$

and (4.5) gives the total tension

$$(4.12) \quad \mathcal{A} = \frac{2}{1 + 24 \sum_{n=1}^{\infty} \left(\int_0^1 H_{\zeta\zeta}(\zeta, 0) \sin(n\pi\zeta) d\zeta \right)^2 e^{-2\tau/n^2\pi^2}}.$$

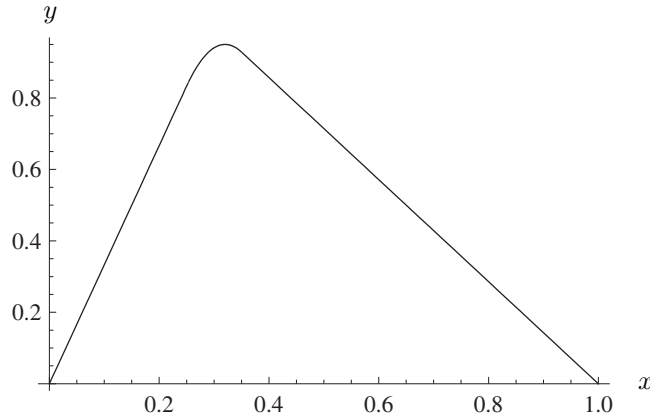


FIG. 4.1. Initial smoothed-corner profile, given by (4.13) with $a = 0.3$, $b = 0.1$, and $H_0 = 1$.

We observe that, as $t \rightarrow \infty$, $H \rightarrow 0$ exponentially, although nonuniformly, with higher modes decaying more slowly. This implies that our model is well posed whether solved forwards or backwards in time. Positive values of τ in (4.8) correspond to the *forward* problem of specifying an initial shape and then following its evolution. Negative values of τ give solutions to the *inverse* problem of specifying the final shape and then determining the required initial condition. This is particularly relevant in the context of glass tube manufacture, where the aim is to find the die shape needed to generate a desired final tube cross-section.

In contrast, two-dimensional surface-tension-driven Stokes flow is certainly ill posed as an inverse problem. This is confirmed in section 6, where we derive the dispersion relation for a viscida of finite thickness and show how the high wavenumbers are eliminated as the inverse aspect ratio tends to zero.

Motivated by the problem of producing glass tubing containing corners, we begin by considering the initial configuration

$$(4.13) \quad H(x, 0) = \begin{cases} \frac{x}{a} H_0, & 0 \leq x \leq a - b/2, \\ \frac{(4ab - 4a^2 + 8a(1 - b)x - (2x - b)^2)}{8ab(1 - a)} H_0, & a - b/2 \leq x \leq a + b/2, \\ \frac{(1 - x)}{1 - a} H_0, & a + b/2 \leq x \leq 1, \end{cases}$$

comprising two straight sections orientated at different angles, with a smooth region joining them of width $b \leq (1 - a)/2$ and center $x = a$, as illustrated in Figure 4.1. The solution (4.8) in this case takes the form

$$(4.14) \quad H = \frac{H_0}{a(1 - a)} \sum_{n=1}^{\infty} \frac{\sin(\frac{1}{2}n\pi b)}{\frac{1}{2}n\pi b} \frac{\sin(n\pi a) \sin(n\pi x)}{n^2\pi^2} e^{-\tau/n^2\pi^2}.$$

We illustrate the effect of decreasing b in Figure 4.2, and observe that doing so causes no significant effect on the global behavior of the viscida. We infer that although

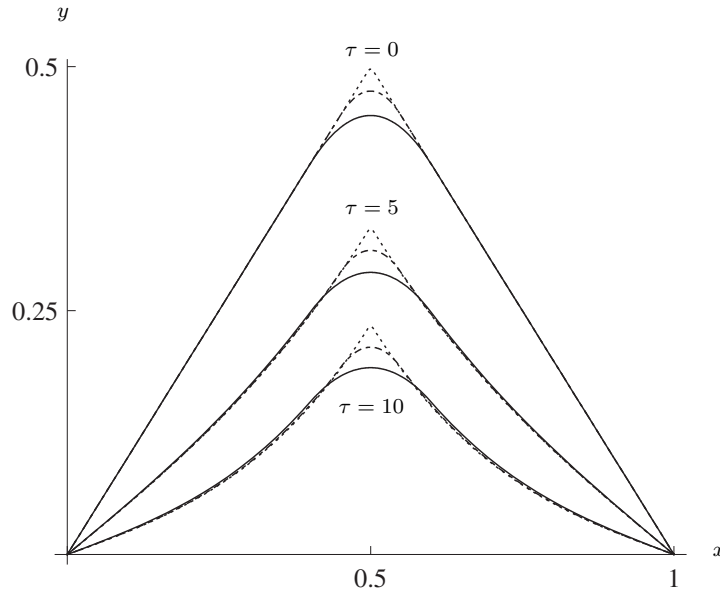


FIG. 4.2. Evolution of the center-line of a simply supported viscida with initial profile given by (4.13) with $H_0 = 1/2$, $a = 1/2$, and $b = 0.1, 0.05, 0.005$ (solid, dashed, and dotted lines, respectively) at $\tau = 0, 5, 10$.

our small-curvature analysis is not applicable near a corner region, it describes the global behavior of an initial configuration containing small regions of high curvature. To obtain the “inner” solution in such regions requires consideration of the full Stokes equations, the matching condition for which would be provided by our “outer” solution.

Reassured by this argument, we henceforth focus only on the initial set-up (4.13) where $b = 0$, and the initial configuration is given by

$$(4.15) \quad H(x, 0) = \begin{cases} \frac{x}{a}H_0, & 0 \leq x \leq a; \\ \frac{1-x}{1-a}H_0, & a \leq x \leq 1. \end{cases}$$

In this case, the solution is simply

$$(4.16) \quad H = -\frac{H_0}{a(1-a)}G(x, a, \tau),$$

with (4.11) and (4.12) giving

$$(4.17) \quad t = \frac{\tau}{6} + \frac{2H_0^2}{a^2(1-a)^2\pi^2} \sum_{n=1}^{\infty} \frac{\sin^2(n\pi a)}{n^2} (1 - e^{-2\tau/n^2\pi^2}),$$

$$(4.18) \quad \mathcal{A} = \frac{2}{1 + \frac{6H_0^2}{a^2(1-a^2)\pi^4} \sum_{n=1}^{\infty} \frac{\sin^2(n\pi a)}{n^4} e^{-2\tau/n^2\pi^2}}.$$

Figure 4.3(a) illustrates the evolution of the viscida center-line given by (4.16) when we choose $a = 1/2$ and $H_0 = 1/2$. We notice that, as time increases, H becomes

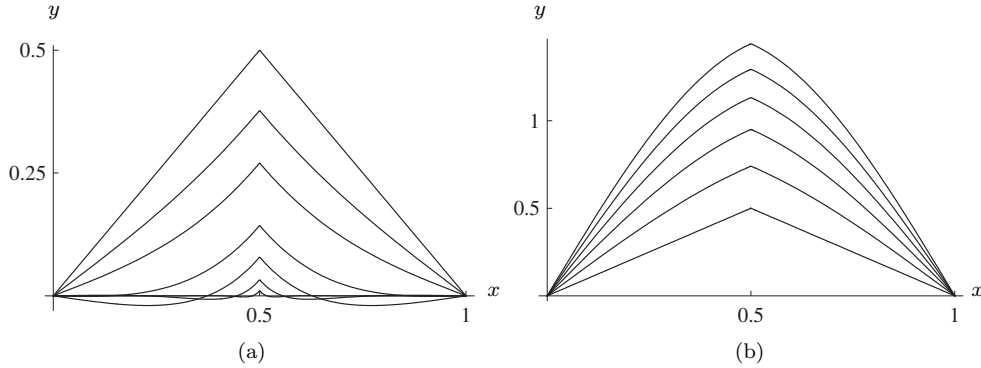


FIG. 4.3. Evolution of the center-line of a simply supported viscida with initial profile given by (4.15) with $H_0 = 1/2$ and $a = 1/2$ for (a) $t = 0, 1, 2, 4, 8, 50, 500$ and (b) $t = 0, -2, -4, -6, -8, -10$.

negative, initially at the extremities as the angle made between the ends and the x -axis passes through zero. This “sagging” feature eventually meets with the competing effect of sheet shrinkage, resulting in the parts of the viscida lying below the x -axis being drawn toward the axis again as the viscida approaches a straight line joining the two ends. As a result, the angle made between the x -axis and the viscida at $x = 0$ increases again. Consequently, there exists a specific time at which a minimum y -value in the viscida is attained (at which time the gradient at $x = 0$ is also a minimum). In addition, as we would expect, the rate of change in the profile evolution decreases as time increases and the profile tends towards the final straight configuration. This is highlighted by the increase in magnitude between consecutive time steps. The corner at $x = a$ appears to persist as the viscida evolves; we investigate this observation further in the following section.

In Figure 4.3(b) the evolution of the profile (4.16) with inverse time is considered. Unlike the forward-time analysis, we take equal time steps, and the sheet length appears to increase at a constant rate. Again, the corner evidently persists; indeed we would not expect a discontinuity in the gradient to appear with forward time if we began with a smooth sheet.

Equation (4.12) shows that the total tension in the sheet is positive for all time, and so (3.12) implies that the leading-order rate of change of sheet length is constrained by the inequality

$$(4.19) \quad -\frac{1}{2} < \frac{dL}{dt} \leq 0.$$

Since dL/dt represents the viscous contribution to the tension in the viscida, we conclude that for large positive time the viscous tension will become negligible and so the surface tension dominates. Conversely, for inverse time the viscous tension will become increasingly negative, tending towards a maximum value equal and opposite to the surface tension contribution as $t \rightarrow -\infty$, so the total sheet tension tends to zero. These features are shown in the graph of \mathcal{A} versus t in Figure 4.4.

4.3. Persistence of the corner. To examine the behavior near the corner we write (4.9) in the form

$$(4.20) \quad G(a + z, a, \tau) = - \sum_{n=1}^{\infty} \frac{\cos(n\pi z)}{n^2\pi^2} e^{-\tau/n^2\pi^2} + \sum_{n=1}^{\infty} \frac{\cos(n\pi(2a + z))}{n^2\pi^2} e^{-\tau/n^2\pi^2},$$

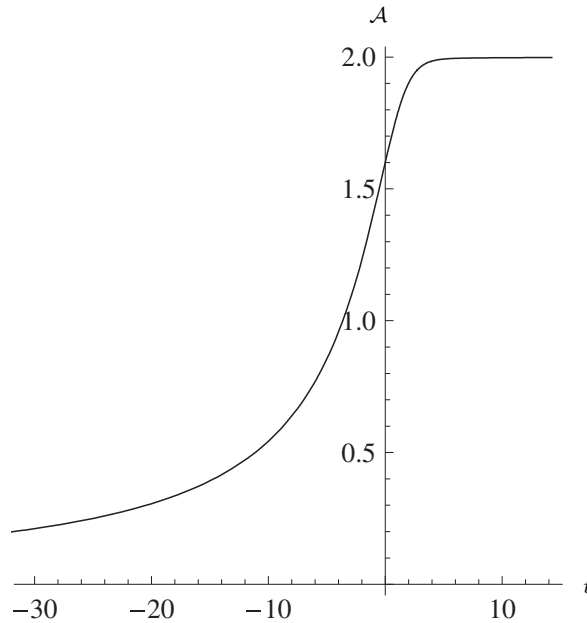


FIG. 4.4. Plot of tension \mathcal{A} versus time t for a simply supported viscida with initial profile given by (4.15) with $H_0 = 1/2$ and $a = 1/2$.

where $z = x - a$. Let us consider the first summation, say, $S(z, \tau)$. Near the corner, $|z| \ll 1$ and we may decompose S into the early terms, where $n = O(1)$ and we can Taylor-expand the cosine, and the late terms where $n = O(1/|z|)$ so we can expand the exponential. Thus we may write

$$\begin{aligned}
 (4.21) \quad S(z, \tau) &\equiv \sum_{n=1}^{\infty} \frac{\cos(n\pi z)}{n^2 \pi^2} e^{-\tau/n^2 \pi^2} \\
 &\sim \sum_{n=1}^{m-1} \left(1 - \frac{n^2 \pi^2 z^2}{2} + O(z^4) \right) \frac{e^{-\tau/n^2 \pi^2}}{n^2 \pi^2} \\
 &\quad + \sum_{n=m}^{\infty} \frac{\cos(n\pi z)}{n^2 \pi^2} \left(1 - \frac{\tau}{n^2 \pi^2} + O(m^{-4}) \right),
 \end{aligned}$$

where m is an integer parameter satisfying $1 \ll m \ll 1/|z|$. The second series in (4.21) may be approximated as an integral using

$$(4.22) \quad \sum_{n=m}^{\infty} f(n\pi|z|) \sim \frac{1}{\pi|z|} \int_{m\pi|z|}^{\infty} f(s) ds + \frac{f(m\pi|z|)}{2} + O(|z|) \quad \text{as } z \rightarrow 0$$

(for suitably integrable f), which implies

$$\begin{aligned}
 (4.23) \quad \sum_{n=m}^{\infty} \frac{\cos(n\pi z)}{n^2 \pi^2} &\sim \frac{|z|}{\pi} \int_{m\pi|z|}^{\infty} \frac{\cos s}{s^2} ds + \frac{\cos(m\pi z)}{2m^2 \pi^2} + \dots \\
 &\sim \frac{1}{\pi^2} \left(\frac{1}{2m^2} + \frac{1}{m} \right) - \frac{|z|}{2} + \left(\frac{m}{2} - \frac{1}{4} \right) z^2 + \dots
 \end{aligned}$$

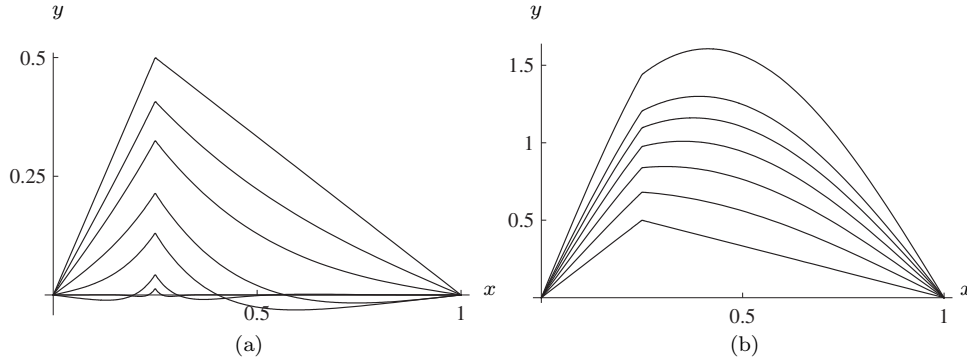


FIG. 4.5. Evolution of the center-line of a simply supported viscida with initial profile given by (4.15) with $H_0 = 1/2$ and $a = 1/4$ for (a) $t = 0, 1, 2, 4, 8, 50, 500$ and (b) $t = 0, -2, -4, -6, -8, -10, -15$.

as $z \rightarrow 0$. Now using this result in (4.21), letting $m \rightarrow \infty$ and $zm \rightarrow 0$, we find that

$$(4.24) \quad S(z, \tau) \sim \sum_{n=1}^{\infty} \frac{e^{-\tau/n^2\pi^2}}{n^2\pi^2} - \frac{|z|}{2} + \frac{z^2}{4} + \frac{z^2}{2} \sum_{n=1}^{\infty} (1 - e^{-\tau/n^2\pi^2}) + O(z^3) \quad \text{as } z \rightarrow 0.$$

When $\tau = 0$, we recognize (4.21) as the 2-periodic Fourier series of the function

$$(4.25) \quad S(z, 0) = \frac{(|z| - 1)^2}{4} - \frac{1}{12}, \quad -1 \leq z \leq 1,$$

and indeed when $\tau = 0$, the first series in (4.24) is equal to $1/6$ and the final series is zero, so (4.24) reproduces (4.25). As τ increases, (4.24) shows that the corner at $z = 0$ is exactly conserved.

Following an identical approach for the second summation in (4.20) provides

$$(4.26) \quad G(a + z, a, \tau) \sim \sum_{n=1}^{\infty} \frac{(\cos(2n\pi a) - 1)}{n^2\pi^2} e^{-\tau/n^2\pi^2} + \frac{|z|}{2} - z \sum_{n=1}^{\infty} \frac{\sin(2n\pi a)}{n\pi} e^{-\tau/n^2\pi^2} + O(z^2)$$

as $z \rightarrow 0$. This shows that the corner singularity in Green's function persists for both forward and inverse time and therefore, using (4.8), that any corners in the profile H will likewise persist for both forward and inverse time. This is true for the solution (4.16) and indeed for any solution of (4.7) with a discontinuity in gradient, since

$$(4.27) \quad \lim_{z \rightarrow 0} [H_{xt}]_{x-z}^{x+z} = \lim_{z \rightarrow 0} \int_{x-z}^{x+z} H \, dx = 0.$$

When $0 < a < 1/2$ for forward time, the second series in (4.26) tends to zero and so the profile rotates such that it becomes locally symmetric about $z = 0$ as shown in Figure 4.5(a). When $a = 1/2$, the second series is identically zero, and continuing the series to $O(z^2)$ in this symmetric case yields

$$(4.28) \quad G \sim -2 \sum_{n=0}^{\infty} \frac{e^{-\tau/(2n+1)^2\pi^2}}{(2n+1)^2\pi^2} + \frac{1}{2}|z| - z^2 \sum_{n=0}^{\infty} (1 - e^{-\tau/(2n+1)^2\pi^2}) + O(|z|^3).$$

Let us examine how the terms in (4.28) behave as $\tau \rightarrow \infty$. The leading term is

$$(4.29) \quad -2 \sum_{n=1}^{\infty} \frac{e^{-\tau/(2n+1)^2\pi^2}}{(2n+1)^2\pi^2} \sim -\frac{1}{\pi\sqrt{\tau}} \int_0^{\infty} \frac{e^{-1/s^2}}{s^2} ds = -\frac{1}{2\sqrt{\pi\tau}},$$

and so the profile height decays algebraically as $\tau \rightarrow \infty$. Similarly, we can estimate the curvature of G at $z = 0$ using

$$(4.30) \quad \sum_{n=0}^{\infty} \left(1 - e^{-\tau/(2n+1)^2\pi^2}\right) \sim \frac{\sqrt{\tau}}{2\pi} \int_0^{\infty} \left(1 - e^{-1/s^2}\right) ds = \frac{1}{2} \sqrt{\frac{\tau}{\pi}}.$$

By substituting (4.29) and (4.30) into (4.28), we see that our small- z approximation becomes nonuniform when $\tau = O(z^{-2})$. Furthermore, as $\tau \rightarrow \infty$, $G \rightarrow 0$ except for a small region near $z = 0$ where the dominant behavior will occur. This motivates us in section 4.4 to seek a uniformly valid approximation for G in the large-time limit.

4.4. Large-time behavior. Motivated by the previous discussion, we perform the rescaling

$$(4.31) \quad z = \frac{\eta}{\sqrt{\tau}}$$

to find a uniformly valid approximation to (4.20) in the large positive-time limit. To lowest order, the second alternating sum may be neglected, and so

$$(4.32) \quad G(x, a, \tau) \sim - \sum_{n=1}^{\infty} \cos\left(\frac{n\pi\eta}{\sqrt{\tau}}\right) \frac{e^{-\tau/n^2\pi^2}}{n^2\pi^2}.$$

The leading-order behavior of (4.32) as $\tau \rightarrow \infty$ is

$$(4.33) \quad G(x, a, \tau) \sim -\frac{f(\eta)}{\sqrt{\tau}},$$

where

$$(4.34) \quad f(\eta) = -\frac{|\eta|}{2} {}_0F_2\left(1, \frac{3}{2}; \frac{\eta^2}{4}\right) + \frac{1}{2\sqrt{\pi}} {}_0F_2\left(\frac{1}{2}, \frac{1}{2}; \frac{\eta^2}{4}\right),$$

and ${}_0F_2$ denotes a generalized hypergeometric function [9].

In Figure 4.6, we compare the asymptotic prediction (4.33) with the exact expression for G from (4.20), expressed in similarity variables, when $a = 1/3$. As predicted in the previous section, G becomes symmetric about $\eta = 0$ and the dominant behavior is confined near to $\eta = 0$. The approximation (4.33) becomes increasingly accurate as τ increases, and the nonsmooth behavior near $\eta = 0$ is captured well. The correct behavior away from $\eta = 0$ is obtained once τ is sufficiently large for the exponentially small corrections to have decayed.

The function $f(\eta)$ goes like

$$(4.35a) \quad f(\eta) \sim \frac{1}{2\sqrt{\pi}} - \frac{|\eta|}{2} \quad \text{as } \eta \rightarrow 0,$$

$$(4.35b) \quad f(\eta) \sim \frac{1}{\sqrt{3\pi}} \exp\left(-\frac{3|\eta|^{2/3}}{2^{5/3}}\right) \cos\left(\frac{3^{3/2}|\eta|^{2/3}}{2^{5/3}}\right) \quad \text{as } \eta \rightarrow \infty.$$

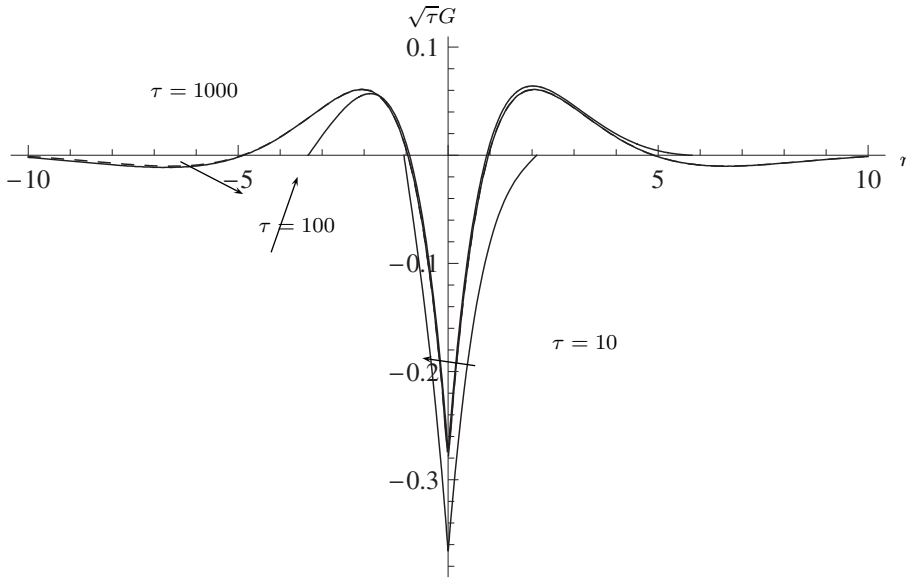


FIG. 4.6. Scaled Green's function $\sqrt{\tau}G(x, a, \tau)$ versus $\eta = \sqrt{\tau}(x - a)$ with $a = 1/3$ and $\tau = 10, 100, 1000$. The function $-f(\eta)$ given by (4.34) is shown as a dashed curve.

Therefore the behavior near the corner is

$$(4.36) \quad G \sim -\frac{1}{2\sqrt{\pi\tau}} + \frac{|x - a|}{2} \quad \text{as } \eta \rightarrow 0 \text{ and } \tau \rightarrow \infty,$$

while for large η , since f decays exponentially, (4.36) is replaced by an exponentially small outer approximation. Equation (4.36) indicates that the magnitude of G decreases algebraically while G becomes symmetric about $x = a$ as $\tau \rightarrow \infty$, and the magnitude of the angle is conserved for large time, corroborating the prediction made by (4.26).

In Figure 4.7 we compare the exact solution for the particular example (4.16) when $H_0 = 1/2$ and $a = 1/2$ with the large positive- τ limit (4.34) when $\tau = 50, 100, 200$. Evidently the behavior near $x = a$ is approximated very well, although the slow decay of $1/\sqrt{\tau}$ means that large values of τ are required to obtain good accuracy across the whole domain.

One interesting prediction of the asymptotic approximation (4.33) is that the viscida will eventually cross the x -axis an infinite number of times as τ increases. We can estimate the number N of zeros of H between (say) $x = 0$ and $x = 1/2$ by counting the zeros of (4.35b) between $\eta = 0$ and $\eta = \sqrt{\tau}/2$, that is,

$$(4.37) \quad N - \frac{1}{2} \sim \frac{3^{3/2}\tau^{1/3}}{2^{7/3}\pi}.$$

This means that the number of zeros grows very slowly with τ ; for example, $\tau \gtrsim 450$ for there to be three zeros.

As $\tau \rightarrow -\infty$, the first term in the series (4.9) dominates, and so

$$(4.38) \quad G(x, a, \tau) \sim -\frac{2 \sin(\pi x) \sin(\pi a)}{\pi^2} e^{-\tau/\pi^2},$$

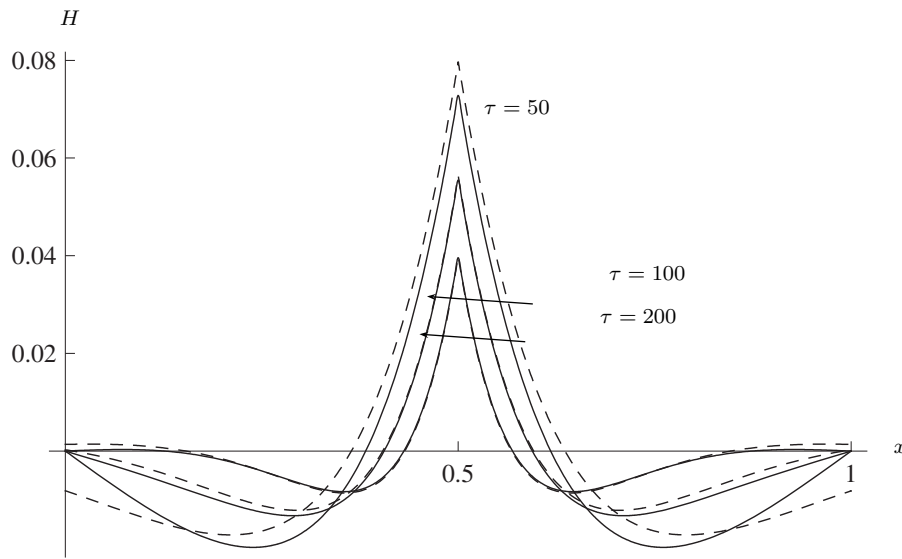


FIG. 4.7. Evolution of a simply supported viscida with initial profile given by (4.15) with $H_0 = 1/2$ and $a = 1/2$ at times $\tau = 50, 100, 200$. The large positive time approximation (4.33) is shown as dashed curves.

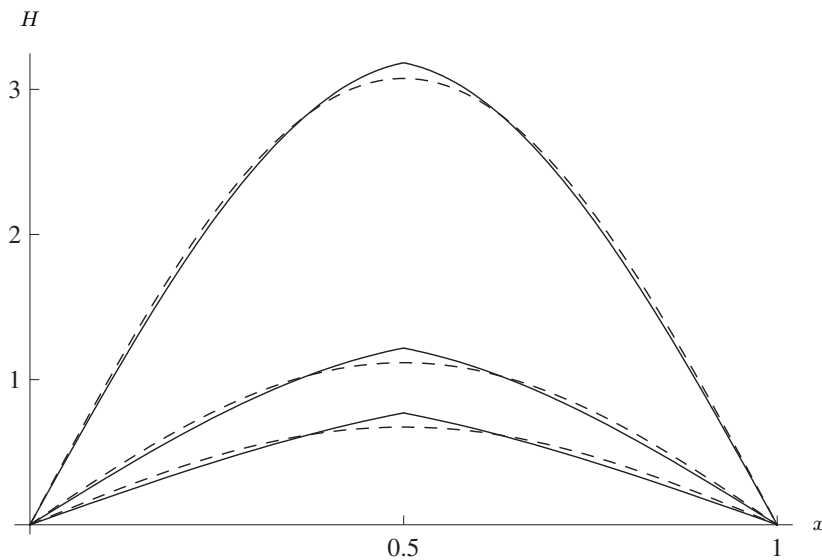


FIG. 4.8. Evolution of a simply supported viscida with initial profile given by (4.15) with $H_0 = 1/2$ and $a = 1/2$ at times $\tau = -5, -10, -20$. The large negative time approximation (4.38) is shown as dashed curves.

which predicts that the profile (4.16) will become symmetric for large negative time, regardless of the value of a . This is indeed observed to be the case when we consider Figures 4.3(b) and 4.5(b). In Figure 4.8 we plot the viscida profile (4.16) with $H_0 = 1/2$ and $a = 1/2$, and compare this to the large negative- τ limit when

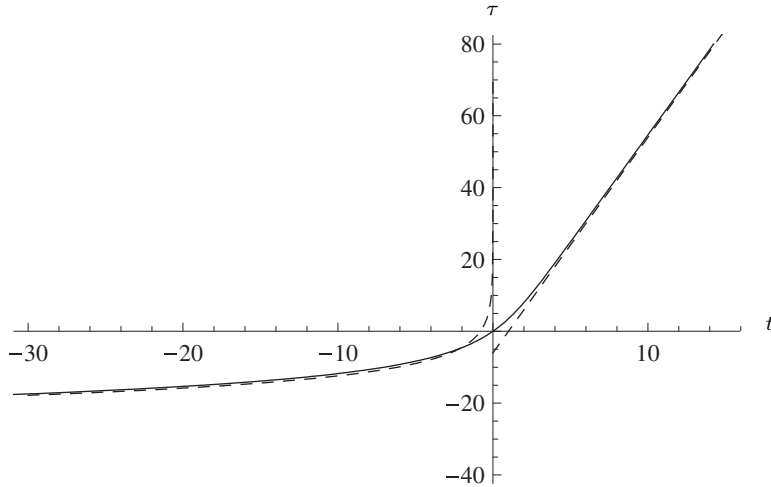


FIG. 4.9. Plot of τ versus t for a simply supported viscida with initial profile given by (4.15) with $H_0 = 1/2$ and $a = 1/2$. The exact result (4.17) is shown as a solid line, while the dashed lines show the asymptotic approximations in the large negative and positive time limits given by (4.39) and (4.40).

$\tau = -5, -10, -20$. We remark on the excellent agreement for relatively small times. However, while (4.38) captures the general profile shape, in discarding the high-wavenumber terms we lose the local information near the corner. For large negative time the corner now represents only a small perturbation to the overall profile. The local behavior near the corner may be captured by a similarity solution in an analogous manner to the large positive-time analysis above.

Analysis of the asymptotic behavior of (4.17) as $t \rightarrow \pm\infty$ gives

$$(4.39) \quad \tau \sim -\frac{\pi^2}{2} \ln \left| \frac{\pi^2 a^2 (1-a)^2 t}{2H_0^2 \sin^2(\pi a)} \right| \quad \text{as } t \rightarrow -\infty,$$

$$(4.40) \quad \tau \sim 6t - \frac{6H_0^2}{a(1-a)} \quad \text{as } t \rightarrow \infty,$$

and so (4.6) implies

$$(4.41) \quad L^{(1)} \sim \frac{H_0^2}{2a(1-a)} - \frac{t}{2} - \frac{\pi^2}{24} \ln \left| \frac{\pi^2 a^2 (1-a)^2 t}{2H_0^2 \sin^2(\pi a)} \right| \quad \text{as } t \rightarrow -\infty,$$

$$(4.42) \quad L^{(1)} \rightarrow 0 \quad \text{as } t \rightarrow \infty.$$

We plot the approximations (4.39) and (4.40) when $H_0 = 1/2$ and $a = 1/2$ alongside the actual result (4.17) in Figure 4.9, and observe good agreement for both forward and inverse time.

4.5. A clamped viscida. We now consider the case where the ends of the viscida are clamped at zero angle, so we must solve (4.3) subject to the fixed-end constraint (3.15) plus the boundary conditions

$$(4.43) \quad H_x(0, \tau) = H_x(1, \tau) = 0.$$

The solution may again be written in the form

$$(4.44) \quad H(x, \tau) = \int_0^1 G(x, \zeta, \tau) H_{\zeta\zeta}(\zeta, 0) \, d\zeta.$$

This time it is convenient to decompose G into parts that are even and odd about $x = 1/2$, that is,

$$(4.45) \quad G(x, \zeta, \tau) \equiv G_e(x, \zeta, \tau) + G_o(x, \zeta, \tau),$$

where G_e and G_o possess the symmetries

$$(4.46a) \quad G_e(1 - x, \zeta, \tau) \equiv G_e(x, \zeta, \tau), \quad G_o(1 - x, \zeta, \tau) \equiv -G_o(x, \zeta, \tau),$$

$$(4.46b) \quad G_e(\zeta, x, \tau) \equiv G_e(x, \zeta, \tau), \quad G_o(\zeta, x, \tau) \equiv G_o(x, \zeta, \tau).$$

Then we find that G_e and G_o are given by

$$(4.47a) \quad G_e(x, \zeta, \tau) = - \sum_{n=1}^{\infty} \frac{2p_n(x)p_n(\zeta)}{n^2\pi^2} e^{-\tau/4n^2\pi^2},$$

$$(4.47b) \quad G_o(x, \zeta, \tau) = - \sum_{n=1}^{\infty} \frac{2q_n(x)q_n(\zeta)}{k_n^4} e^{-\tau/k_n^2},$$

where

$$(4.48) \quad p_n(x) = \sin^2(n\pi x), \quad q_n(x) = k_n(1 - 2x) + 2 \sin(k_n x) - k_n \cos(k_n x),$$

and the eigenvalues k_n are the positive solutions of the transcendental equation

$$(4.49) \quad \tan\left(\frac{k_n}{2}\right) = \frac{k_n}{2}.$$

The relation between τ and t is given by (4.2) as

$$(4.50) \quad t = \frac{\tau}{6} + 2 \sum_{n=1}^{\infty} \left(\int_0^1 H_{\zeta\zeta}(\zeta, 0) p_n(\zeta) \, d\zeta \right)^2 \frac{(1 - e^{-\tau/2n^2\pi^2})}{n^2\pi^2} + 2 \sum_{n=1}^{\infty} \left(\int_0^1 H_{\zeta\zeta}(\zeta, 0) q_n(\zeta) \, d\zeta \right)^2 \frac{(1 - e^{-2\tau/k_n^2})}{k_n^4},$$

while (4.5) provides the tension

$$(4.51) \quad \mathcal{A} = 2 \left[1 + 6 \sum_{n=1}^{\infty} \left(\int_0^1 H_{\zeta\zeta}(\zeta, 0) p_n(\zeta) \, d\zeta \right)^2 \frac{e^{-\tau/2n^2\pi^2}}{n^4\pi^4} + 4 \sum_{n=1}^{\infty} \left(\int_0^1 H_{\zeta\zeta}(\zeta, 0) q_n(\zeta) \, d\zeta \right)^2 \frac{e^{-2\tau/k_n^2}}{k_n^8} \right]^{-1}.$$

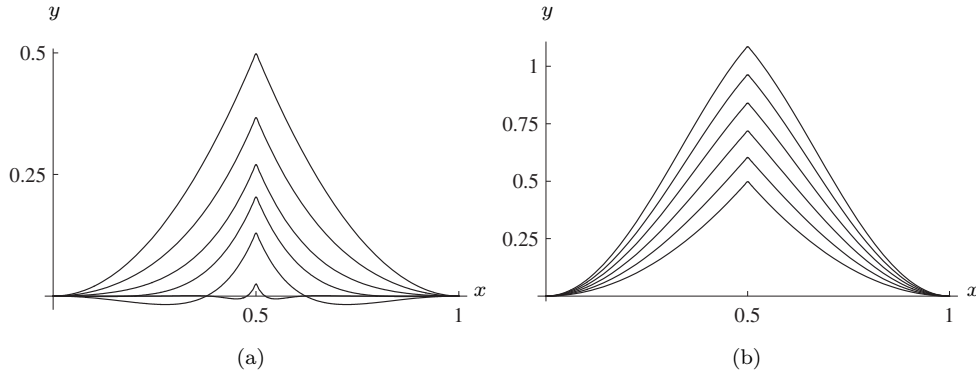


FIG. 4.10. Evolution of the center-line of a clamped viscida with initial profile given by (4.52) with $H_0 = 1/2$ and $a = 1/2$ for (a) $t = 0, 3, 6, 9, 15, 30, 300$ and (b) $t = 0, -2, -4, -6, -8, -10$.

We consider the initial profile

$$(4.52) \quad H(x, 0) = \begin{cases} \frac{x^2}{a^2}H_0, & 0 \leq x \leq a; \\ \frac{(x-1)^2}{(a-1)^2}H_0, & a \leq x \leq 1, \end{cases}$$

which satisfies the clamped-end conditions (4.43) while replicating corner behavior at $x = a$. In the symmetric case when $a = 1/2$, G_o is identically zero and only the symmetric part G_e contributes. Here (4.44) is simply

$$(4.53) \quad H(x, \tau) = -8H_0 \sum_{n=1}^{\infty} \frac{(-1)^n \sin^2(n\pi x)}{n^2\pi^2} e^{-\tau/4n^2\pi^2},$$

while the relation between τ and t , (4.50), is

$$(4.54) \quad t = \frac{\tau}{6} + 32H_0^2 \sum_{n=1}^{\infty} \frac{(1 - e^{-\tau/2n^2\pi^2})}{n^2\pi^2},$$

and the tension (4.51) reads

$$(4.55) \quad \mathcal{A} = \frac{2}{1 + 96H_0^2 \sum_{n=1}^{\infty} \frac{e^{-\tau/2n^2\pi^2}}{n^4\pi^4}}.$$

The evolution of such a symmetric profile is displayed in Figure 4.10. We observe analogous behavior to the simply supported profile, specifically persistence of the corner and well posedness for inverse time.

Initial profiles whose ends are fixed at nonzero angle can also be represented in the form (4.44) with G given by (4.45). Indeed, local analysis of G near $x = 0$ and $x = 1$ reveals that

$$(4.56) \quad G(x, a, \tau) \sim -\frac{(1-a)x}{2} + O(x^2) \quad \text{for } x \ll 1,$$

$$(4.57) \quad G(x, a, \tau) \sim \frac{a(x-1)}{2} + O((1-x)^2) \quad \text{for } 1-x \ll 1,$$

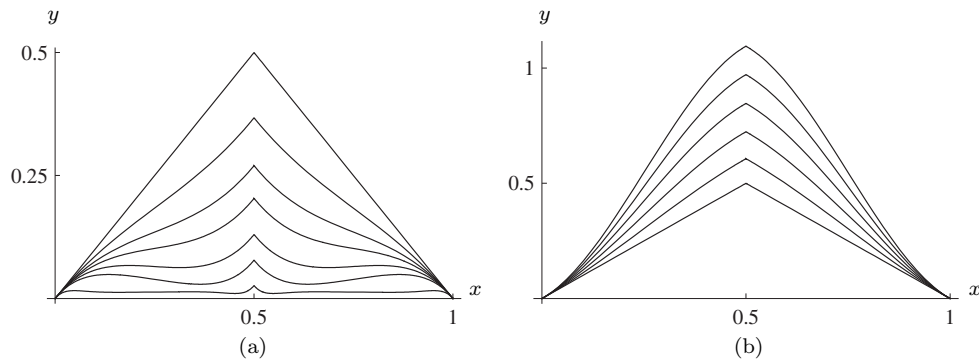


FIG. 4.11. Evolution of the center-line of a clamped viscida with initial profile given by (4.15) with $H_0 = 1/2$ and $a = 1/2$ for (a) $t = 0, 3, 6, 9, 15, 30, 300$ and (b) $t = 0, -2, -4, -6, -8, -10$.

which implies that the angle at each end is conserved. The fact that the separable solution may represent a solution which satisfies inhomogeneous clamped-end conditions is a result of the Gibbs phenomenon.

This result allows us to reconsider the initial corner profile (4.15), for which (4.44) gives

$$(4.58) \quad H = -\frac{H_0}{a(1-a)}G(x, a, \tau),$$

with G given by (4.45), while (4.2) gives

$$(4.59) \quad t = \frac{\tau}{6} + \frac{2H_0^2}{a^2(1-a)^2} \sum_{n=1}^{\infty} \frac{p_n(a)^2}{n^2\pi^2} \left(1 - e^{-\tau/2n^2\pi^2}\right) + \sum_{n=1}^{\infty} \frac{q_n(a)^2}{k_n^4} \left(1 - e^{-2\tau/k_n^2}\right).$$

This provides the evolution of the initial corner profile (4.15) considered in section 4.2 when we fix the angles at each end. In Figure 4.11 we investigate the evolution of such a profile when $H_0 = 1/2$ and $a = 1/2$. Unlike the simply supported set-up, the profile now remains entirely above the x -axis for all time, and we also find that evolution towards the final state occurs more slowly.

As we approach the large positive-time limit, the profile still tends towards a straight line, but since the clamped-end boundary conditions are not satisfied by such a state, we observe the appearance of inner regions near the ends where the curvature is not small and near the center where the corner is maintained. We will show below how the local behavior of our model can be analyzed in these regions as in sections 4.3 and 4.4.

The tension in the sheet is

$$(4.60) \quad \mathcal{A} = \frac{2}{1 + \frac{2H_0^2}{a^2(1-a)^2} \sum_{n=1}^{\infty} \frac{3p_n(a)^2 e^{-\tau/2n^2\pi^2}}{n^4\pi^4} + \frac{2q_n(a)^2 e^{-2\tau/k_n^2}}{k_n^8}}$$

and is plotted in Figure 4.12 for the case when $H_0 = 1/2$ and $a = 1/2$. Qualitatively similar behavior to the case where the ends were simply-supported is displayed, although variations occur more slowly, for both forward and inverse time.

4.6. Persistence of the corner. A similar procedure to the simply supported analysis in section 4.3 provides an expression for $G(x, a, \tau)$ local to $x = a$, namely,

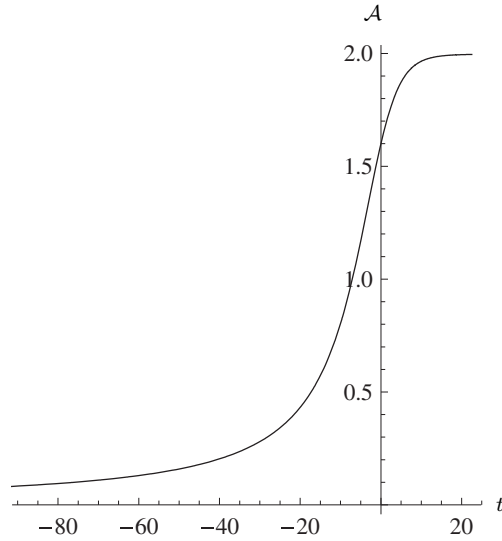


FIG. 4.12. Plot of tension \mathcal{A} versus time t for a clamped viscida with initial profile given by (4.15) with $H_0 = 1/2$ and $a = 1/2$.

$$\begin{aligned}
 G(a - z, a, \tau) &\sim \sum_{n=1}^{\infty} (\cos(4n\pi a) + 4 \cos(2n\pi a) - 3) \frac{e^{-\tau/4n^2\pi^2}}{4n^2\pi^2} \\
 &+ \sum_{n=1}^{\infty} 2 [k_n(1 - 2a) + 2 \sin(k_n a) - k_n \cos(k_n a)]^2 e^{-\tau/k_n^2} - \frac{|z|}{4} \\
 &+ z \sum_{n=1}^{\infty} \frac{2}{k_n^3} (k_n(1 - 2a) + 2 \sin(k_n a) - k_n \cos(k_n a)) [2 \cos(k_n a) + k_n \sin(k_n a)] e^{-\tau/k_n^2} \\
 &+ O(z^2),
 \end{aligned}
 \tag{4.61}$$

where $z = x - a$ and $|z| \ll 1$. Hence the corner again persists for both forward and inverse time. For the initial configuration (4.15) when $0 < a < 1/2$ we observe similar behavior to the simply supported profile, namely, evolution towards a symmetric configuration near the corner for positive time as the corner rotates, and formation of a symmetric profile for large negative time. In Figure 4.13 we consider the evolution of the initial profile (4.15) when $H_0 = 1/2$ and $a = 1/4$.

When $a = 1/2$, since $G_o(x, 1/2, \tau) \equiv 0$, only G_e contributes so the third series in (4.61) is identically zero. This indicates that for symmetric profiles given by (4.15) the corner is exactly conserved as was observed in Figure 4.11.

4.7. Large-time approximation. We can use trigonometric identities to write (4.47a) in the form

$$\begin{aligned}
 (4.62) \quad G_e(x, a, \tau) &= \sum_{n=1}^{\infty} \left\{ -2 + 2 \cos(2n\pi x) + 2 \cos(2n\pi a) \right. \\
 &\quad \left. - \cos(2n\pi(x - a)) - \cos(2n\pi(x + a)) \right\} \frac{e^{-\tau/4n^2\pi^2}}{4n^2\pi^2}.
 \end{aligned}$$

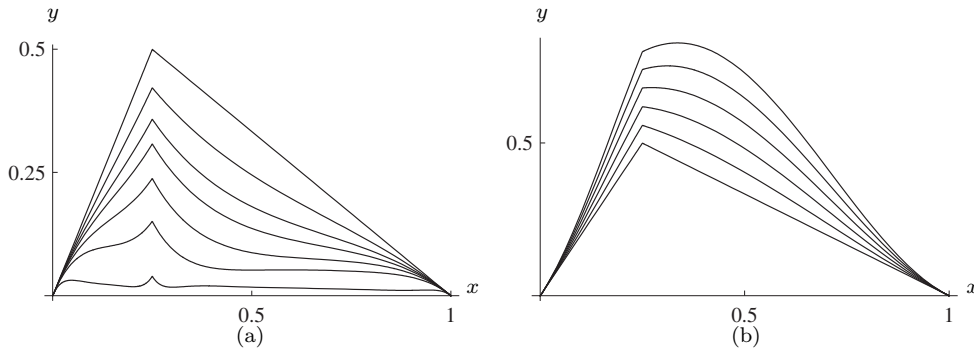


FIG. 4.13. Evolution of the center-line of a clamped viscida with initial profile given by (4.15) with $H_0 = 1/2$ and $a = 1/4$ for (a) $t = 0, 3, 6, 9, 15, 30, 300$ and (b) $t = 0, -2, -4, -6, -8, -10$.

For G_o , the early terms in the series (4.47b) are exponentially small as $\tau \rightarrow \infty$, and we can simplify the later terms using the approximation

$$(4.63) \quad k_n \sim (2n + 1)\pi + O(1/n) \quad \text{as } n \rightarrow \infty,$$

and so, just retaining the leading-order terms, we obtain

$$(4.64) \quad G_o \sim -2 \sum_{n=0}^{\infty} \frac{[1 - 2x - \cos((2n + 1)\pi x)] [1 - 2a - \cos((2n + 1)\pi a)]}{(2n + 1)^2 \pi^2} e^{-\tau/(2n+1)^2 \pi^2}$$

as $\tau \rightarrow \infty$. The leading-order behavior of (4.62) and (4.64) as $\tau \rightarrow \infty$ can now be inferred in a similar manner to the simply supported case.

We begin by considering the simpler case when $a = 1/2$ and only G_e contributes. We also suppose, without loss of generality, that x lies in the interval $[0, 1/2]$; the symmetries (4.46) may then be used to extend our results into $x > 1/2$. If $0 < x < 1/2$, then the cosines contribute exponentially small terms to the series (4.62), while the leading term (independent of x and a) gives

$$(4.65) \quad G(x, 1/2, \tau) \sim - \sum_{n=1}^{\infty} \frac{e^{-\tau/4n^2 \pi^2}}{4n^2 \pi^2}.$$

When x is close to zero, the first cosine in (4.62) becomes nonnegligible, while, recalling that we are only considering the case $a = 1/2$ here, we see that the final two cosines in (4.62) are equal and significant when x is close to $1/2$. We therefore obtain

$$(4.66) \quad G(x, 1/2, \tau) \sim \sum_{n=1}^{\infty} \left\{ -1 + \cos(2n\pi x) - \cos(2n\pi(x - a)) \right\} \frac{e^{-\tau/4n^2 \pi^2}}{2n^2 \pi^2}.$$

Using similar techniques to section 4.3, we can write (4.66) as

$$(4.67) \quad G(x, 1/2, \tau) \sim -\frac{1}{\sqrt{\tau}} \left\{ \frac{1}{2\sqrt{\pi}} - f(x\sqrt{\tau}) + f((1/2 - x)\sqrt{\tau}) \right\}$$

as $\tau \rightarrow \infty$, where f is again defined by (4.34).

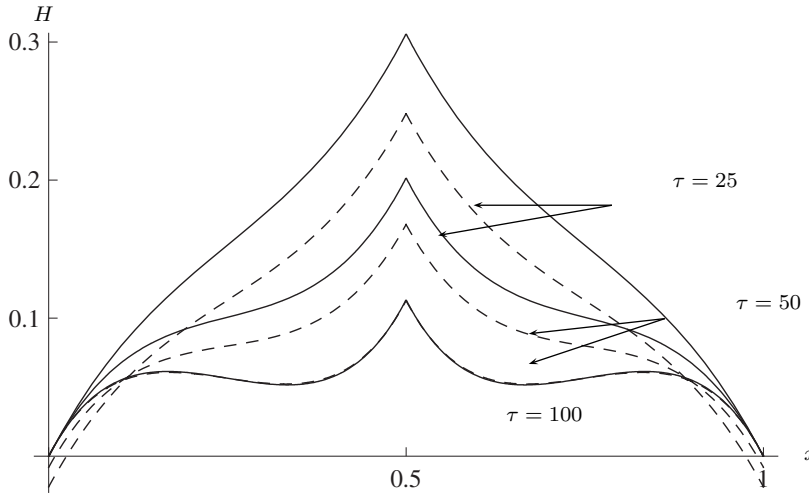


FIG. 4.14. Viscida center-line $H(x, \tau)$ versus x given by (4.58) with $H_0 = 1/2$, $a = 1/2$, and clamped boundary conditions at $\tau = 25, 50, 100$. The asymptotic approximation (4.67) is shown as dashed curves.

We compare (4.67) with the exact solution for the particular profile (4.58) when $H_0 = 1/2$ and $a = 1/2$ in Figure 4.14. We see again that it takes some time for the exponentially small corrections to decay, but, by $\tau = 100$, the exact and approximate solutions are virtually indistinguishable. The asymptotic structure in this case is of outer regions, where H is approximately spatially uniform, matched to inner regions near the clamped ends and the corner at the center, where the gradient changes rapidly.

Following a similar procedure for the case when $a \neq 1/2$, we find that G may be approximated by

$$\begin{aligned}
 G \sim & \frac{(x + a - xa)}{\sqrt{\pi\tau}} + \frac{(1 - 2x)}{\sqrt{\tau}} f(a\sqrt{\tau}) - \frac{2(1 - a)}{\sqrt{\tau}} f((1 - a)\sqrt{\tau}) \\
 & + \frac{2(1 - a)}{\sqrt{\tau}} f(x\sqrt{\tau}) - \frac{2(1 - a)}{\sqrt{\tau}} f((1 - x)\sqrt{\tau}) - \frac{f((x + a)\sqrt{\tau})}{2\sqrt{\tau}} \\
 (4.68) \quad & + \frac{f((1 - x + a)\sqrt{\tau})}{2\sqrt{\tau}} - \frac{f(|x - a|\sqrt{\tau})}{\sqrt{\tau}}.
 \end{aligned}$$

The properties of $f(\eta)$ as $\eta \rightarrow 0$ and $\eta \rightarrow \infty$, given by (4.35), indicate that

$$(4.69) \quad G \sim \frac{(a - 1)}{2\sqrt{\pi\tau}} - \frac{|x - a|}{2} \quad \text{as } x \rightarrow a \text{ and } \tau \rightarrow \infty$$

and therefore predicts that, as in the simply supported case, the magnitude of the angle is conserved for large time.

Figure 4.15 shows the approximate profile predicted by (4.68) for the initial configuration (4.15) with $H_0 = 1/2$ and $a = 1/4$. The approximation is not as accurate for smaller times as the symmetric case; however, when τ is suitably large, the approximate and exact solutions still lie very close together.

For large negative time, the first term in the series (4.47a) dominates, thus predicting that any initial configuration given by (4.58) will approach a symmetric final

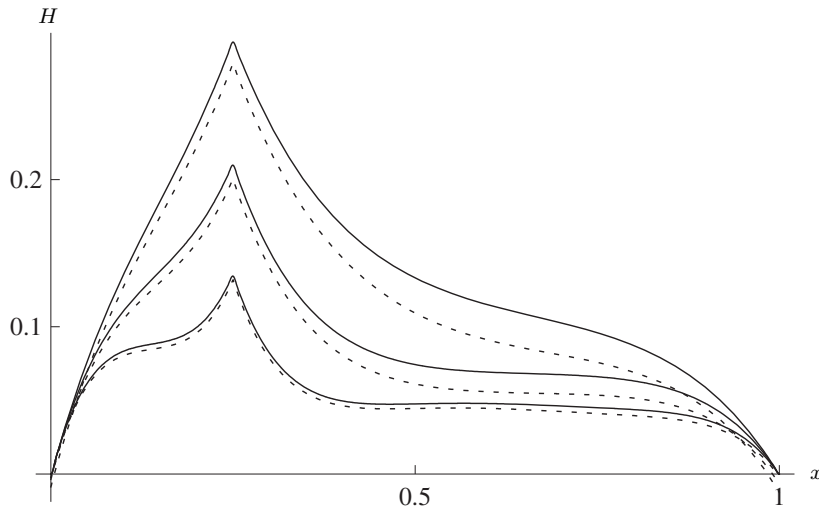


FIG. 4.15. Viscida center-line $H(x, \tau)$ versus x given by (4.58) with $H_0 = 1/2$, $a = 1/4$, and clamped boundary conditions at $\tau = 50, 100, 200$. The asymptotic approximation (4.67) is shown as dashed curves.

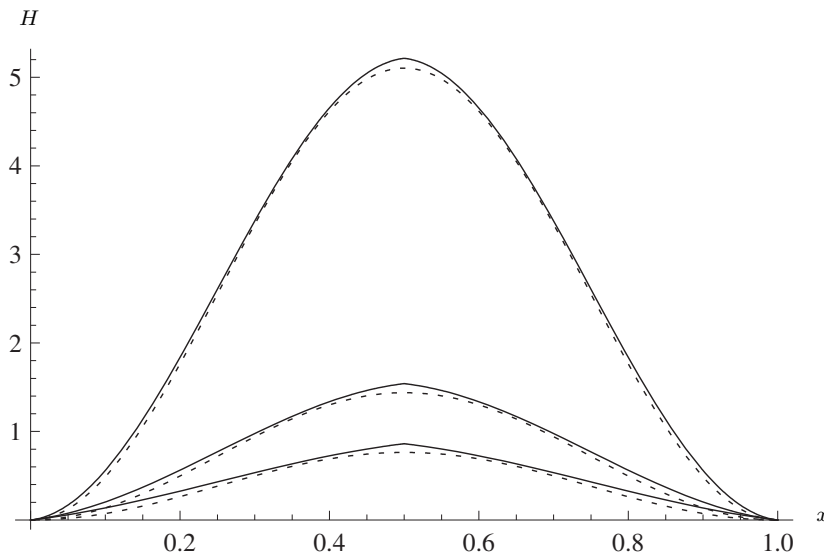


FIG. 4.16. Viscida center-line $H(x, \tau)$ versus x given by (4.58) with $H_0 = 1/2$, $a = 1/2$, and clamped boundary conditions at $\tau = -25, -50, -100$. The approximation where we retain only the first term in (4.47a) is shown as dashed curves.

state. The approximation to H when $a = 1/2$ where we retain only the first term in the series is shown in Figure 4.16. We observe good agreement as τ becomes large, although it now takes longer for the approximate and exact expression to converge than for the simply supported profile. This is because the clamped-end boundary condition is not satisfied by the asymptotic approximation where we retain only the first term in the series. Again, by retaining only the first term in the series (4.47a), we lose the local information near the corner.

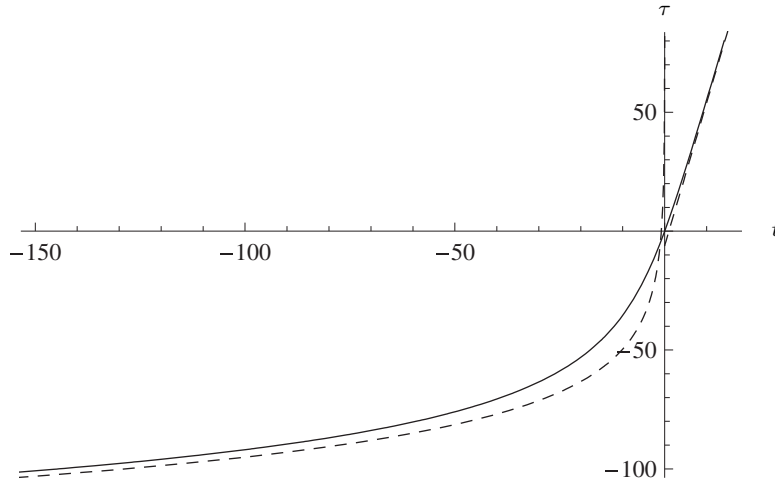


FIG. 4.17. Plot of τ versus t for a clamped viscida with initial profile given by (4.15) with $H_0 = 1/2$ and $a = 1/2$. The solid line shows the exact result (4.59), while the dashed lines show the large positive and negative time asymptotic approximations given by (4.70) and (4.74).

We may examine the asymptotic limits of (4.59) and (4.6). In the large positive-time limit we obtain

$$(4.70) \quad \tau \sim 6t - \frac{6H_0^2}{a(1-a)} - \frac{12H_0^2}{a^2(1-a)^2\pi^2} \sum_{n=1}^{\infty} \frac{q_n(a)^2}{k_n^4} \quad \text{as } t \rightarrow \infty,$$

$$(4.71) \quad L^{(1)} \sim -\frac{H_0^2}{a^2(1-a)^2\pi^2} \sum_{n=1}^{\infty} \frac{q_n(a)^2}{k_n^4} \quad \text{as } t \rightarrow \infty.$$

In the large negative-time limit there are two cases. If $a \neq 1/2$, then

$$(4.72) \quad \tau \sim -k_1 \ln \left(\frac{a(1-a)k_1^2|t|^{1/2}}{\sqrt{2}H_0q_1(a)} \right) \quad \text{as } t \rightarrow -\infty,$$

$$(4.73) \quad L^{(1)} \sim \frac{H_0^2}{2a(1-a)} - k_1 \ln \left(\frac{a(1-a)k_1^2|t|^{1/2}}{\sqrt{2}H_0q_1(a)} \right) - \frac{t}{2} \quad \text{as } t \rightarrow -\infty,$$

but if $a = 1/2$, since $q_1(1/2) = 0$, the limit in this case is

$$(4.74) \quad \tau \sim -4\pi^2 \ln \left(\frac{\pi|t|^{1/2}}{4\sqrt{2}H_0} \right) \quad \text{as } t \rightarrow -\infty,$$

$$(4.75) \quad L^{(1)} \sim 2H_0^2 - \frac{\pi^2}{3} \ln \left(\frac{\pi|t|^{1/2}}{4\sqrt{2}H_0} \right) - \frac{t}{2} \quad \text{as } t \rightarrow -\infty.$$

We plot the relation between τ and t , (4.59), and the asymptotic approximations as $t \rightarrow \pm\infty$ when $a = 1/2$, (4.70) and (4.74), in Figure 4.17. We observe that the agreement for positive time is again excellent, although the approximation for negative time is less accurate than for the simply supported viscida.

5. Nonzero applied pressure.

5.1. A simply supported profile. We now examine the effect of applying a constant pressure difference across the viscida. In particular, we are interested in whether the corner is still maintained in this situation and to what extent a pressure difference offers control over the viscida evolution.

Applying the fixed-end and simple-support boundary conditions, (3.15) and (3.16), respectively, we may integrate the governing equation (3.13) to give

$$(5.1) \quad \frac{1}{3}H_{xxt} = \mathcal{A}H + \frac{Px(x-1)}{2},$$

where \mathcal{A} is again related to H by (3.12).

The change of variable (4.1) no longer provides the decoupling of (3.12) and (5.1) that was achieved when P was zero. In addition, \mathcal{A} is no longer strictly positive, and so (4.1) does not represent a one-to-one relation. However, we do find that the function $\tau(t)$ still appears in the solution.

Seeking a separable solution to (5.1) gives

$$(5.2) \quad H = \sum_{n=1}^{\infty} f_n(t) \sin(n\pi x),$$

where

$$(5.3) \quad f_n(t) = \left[a_n + \frac{6P(1 - (-1)^n)}{n^5\pi^5} \int_0^t e^{\tau(s)/n^2\pi^2} ds \right] e^{-\tau(t)/n^2\pi^2},$$

with the a_n determined by the initial condition. Equation (4.2) then gives an implicit relation for $\tau(t)$, namely,

$$(5.4) \quad t = \frac{\tau}{6} + \sum_{n=1}^{\infty} \frac{n^2\pi^2 a_n^2}{2} - \left[a_n + \frac{6P(1 - (-1)^n)}{n^5\pi^5} \int_0^t e^{\tau(s)/n^2\pi^2} ds \right]^2 \frac{n^2\pi^2 e^{-2\tau(t)/n^2\pi^2}}{2}.$$

Unlike the unpressurized case, t and τ are now related by an integral equation. Once $\tau(t)$ is determined, the viscida profile is given by (5.2), while the tension is given by

$$(5.5) \quad \mathcal{A}(t) = \frac{2 + 24P \sum_{n=0}^{\infty} \frac{f_{2n+1}(t)}{(2n+1)^3\pi^3}}{1 + 6 \sum_{n=1}^{\infty} f_n(t)^2}.$$

While we have demonstrated that, in principle, the solution may be obtained in a similar manner to that considered when $P = 0$, practically this is quite arduous to implement. Therefore for further analysis we solve (5.1) numerically.

By integrating (5.1) and using (3.15) and (3.16), we obtain

$$(5.6) \quad H_t = 3\mathcal{A} \left[\int_0^x (x-s)H(s,t) ds - x\overline{(1-x)H} \right] + \frac{1}{8}Px(x-1)(x^2 - x - 1),$$

and (3.12) gives

$$(5.7) \quad \mathcal{A} = \frac{2 + 6P\overline{x(1-x)H}}{1 + 12\overline{H^2}},$$

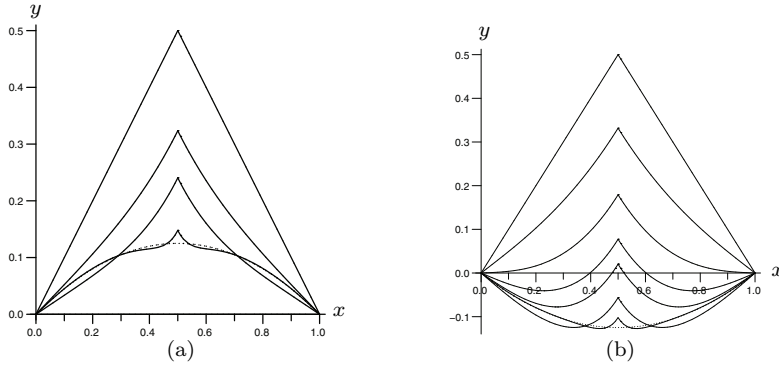


FIG. 5.1. Evolution of a simply supported viscida with initial profile given by (4.15) with $H_0 = 1/2$ and $a = 1/2$ for (a) $P = 2$, $t = 0, 1, 2.5, 5, 100$ and (b) $P = -2$, $t = 0, 1, 2, 3, 4, 20, 100$. In both cases the asymptotic solution (5.9) is shown as a dotted line.

where we define the average of any function $\varphi(x, t)$ by

$$(5.8) \quad \bar{\varphi}(t) = \int_0^1 \varphi(x, t) dx.$$

Now we can evaluate \mathcal{A} at each instant using (5.7) and then use (5.6) to update H . The problem is extremely stable, and we obtained excellent convergence using an explicit Euler time-stepping scheme.

Upon considering steady solutions of the system (3.12) and (5.1), we find that the order reduces by two, and there exists a unique nontrivial steady solution which satisfies the fixed-end constraint (3.15), namely,

$$(5.9) \quad H(x) = \frac{P}{4}x(1 - x).$$

This is the leading-order equivalent of a constant-curvature profile, and, when $P < 0$, is the shape assumed by a small-curvature viscida sagging under the influence of gravity [10].

In Figure 5.1 we consider the forward time evolution of an initial corner profile given by (4.15) with $H_0 = 1/2$ and $a = 1/2$, under positive and negative applied pressures, which correspond to pressurizing the viscida from below or above, respectively. The primary difference from the unpressurized case (Figure 4.3) is that the viscida no longer relaxes to a straight line but instead evolves towards the steady solution (5.9) as $t \rightarrow \infty$. We note, however, that, for the initial profile (4.15), $H_{xx}(x, 0) = H_{xx}(1, t) = 0$, while $H_{xx}(x) = -P/2$ for (5.9), and so the simple-support conditions (3.16) are satisfied only in the case when $P = 0$. When P is nonzero, the profile tends towards the steady solution (5.9) except in a small region near each end, where the viscida must satisfy the simply supported boundary conditions (3.16), and near the corner at $x = a$. These small regions can be analyzed in a manner analogous to section 4.3. Despite this, we observe that (5.9) is an excellent approximation to the final profile configuration, even near the ends.

The persistence of the corner is still clearly evident for both positive and negative time. Application of a negative pressure now allows the entire sheet to lie below the x -axis after a given time. We also notice that the applied pressure acts with the surface-tension effects to accelerate the evolution of the profile towards its final configuration.

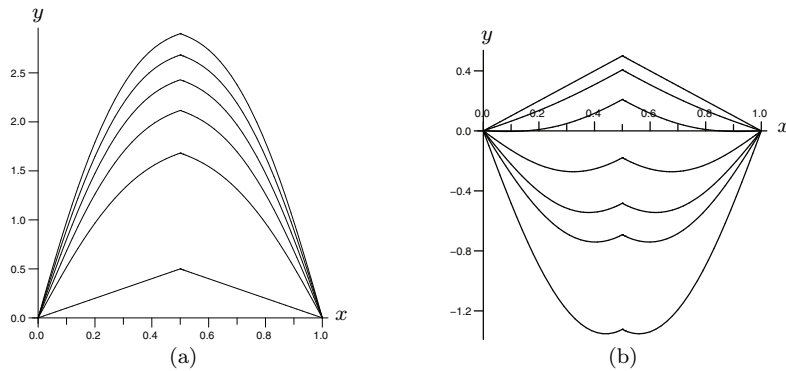


FIG. 5.2. Inverse time evolution of a simply supported viscida with initial profile given by (4.15) with $H_0 = 1/2$, $a = 1/2$, and (a) $P = -100$, $t = 0, -2, -4, -6, -8, -10$, (b) $P = 10$, $t = 0, -1, -2, -3, -4, -5, -10$.

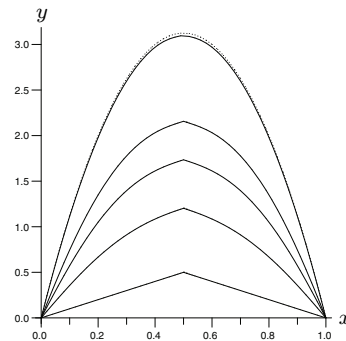


FIG. 5.3. Time evolution of a simply supported viscida with initial profile given by (4.15) with $H_0 = 1/2$, $a = 1/2$, and $P = 50$, $t = 0, 2.5, 10, 25, 50, 400$. The asymptotic solution (5.9) is shown as a dotted line.

In Figure 5.2 we show the influence of an applied pressure on inverse time evolution. In Figure 5.2(a) we consider a negative applied pressure $P = -100$, which we choose to be quite large to have a noticeable influence on the evolution. The main difference we observe is that, although the shape evolution is similar, the timescale over which it occurs is shorter since the applied pressure is also acting to evolve the viscida. We also notice that the viscida appears to evolve towards a smoother profile, with constant curvature, in an analogous manner to the forward time evolution. The profile does not relax to a steady configuration though, but instead the length continues to increase. In Figure 5.2(b) we apply a positive pressure, and similarly, the viscida length continues to increase with time. The extent of the region over which the corner persists again appears to decrease as t becomes increasingly negative. Comparing Figure 5.2(a) with Figure 5.3, we notice a qualitative similarity between forward time evolution with positive pressure and inverse time evolution with a negative pressure.

The influence of the applied pressure on sheet tension is displayed in Figure 5.4. Under positive pressurization, the initial tension increases with increasing pressure. We find that, for sufficiently large pressure, namely, $P \approx 6.0$, the tension is no longer bounded between the large positive- and negative-time asymptotes but now attains maximum and minimum values at specific finite times t_{\max} and t_{\min} , respectively,

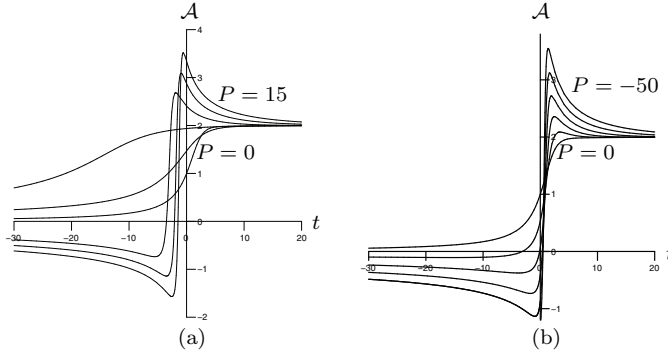


FIG. 5.4. Plot of \mathcal{A} versus t for a simply supported viscida with initial profile given by (4.15) with $H_0 = 1/2$, $a = 1/2$, and (a) $P = 0, 3, 6, 9, 12, 15$, (b) $P = 0, -10, -20, -30, -40, -50$.

whose magnitudes increase with increasing pressure. For all cases though, the tension still tends towards the same limits as the unpressurized case as $t \rightarrow \pm\infty$, namely, 2 and 0.

The influence of a negative applied pressure displays many of the same features, in particular increasing extrema with increasing pressure. However, for a given magnitude in pressure, the variation in tension is more concentrated near $t = 0$. This is reflected in the profile evolution, where viscida motion clearly occurs more quickly under negative pressure. As P becomes increasingly negative, the tension at $x = 0$ decreases. The fact that the tensions are larger for forward time and smaller for inverse time when $P \neq 0$ concurs with the observation that the evolution under applied pressure will occur on a faster timescale than when no pressure is applied. We find that local extrema occur for all values of $P < 0$.

The result that for negative time the tension may now be negative is especially interesting. This means that the viscous contribution to the total tension is no longer constrained to being equal and opposite in magnitude to the surface-tension contribution, and the viscida changes from being under tension to under compression. Note that the applied pressure causes the profile to continue evolving even when the tension in the sheet is zero.

5.2. A clamped viscida. We now investigate the effect of applied pressure on a clamped viscida. Integration of (3.13) and application of (3.15) and (3.17) allows us to write the system as

$$(5.10) \quad H_t = 3\mathcal{A} \left[\int_0^x (x-s)H \, ds + (2x-3)x^2\overline{(1-x)H} \right] - 3x^2(x-1)\overline{H}\mathcal{A} + \frac{P}{8}x^2(x-1)^2,$$

with

$$(5.11) \quad \mathcal{A} = \frac{2 - \overline{(6x^2 - 6x + 1)HP}}{1 + 12 \left[\overline{H^2} - \overline{H}^2 - 3(\overline{H} - 2x\overline{H})^2 \right]},$$

which may again be solved via a time-stepping scheme. As discussed earlier, (5.9) is a steady solution of (3.13) subject to (3.15), but for this solution, $H_x = P/4$ at

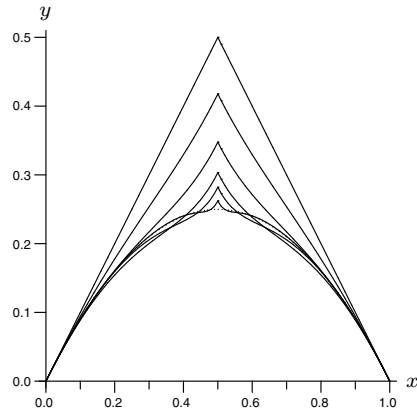


FIG. 5.5. Forward time evolution of a clamped viscida with initial profile given by (4.15) with $H_0 = 1/2$, $a = 1/2$, and $P = 4$ for $t = 0, 4, 10, 20, 100, 400$. The asymptotic solution (5.9) is shown as a dotted line.

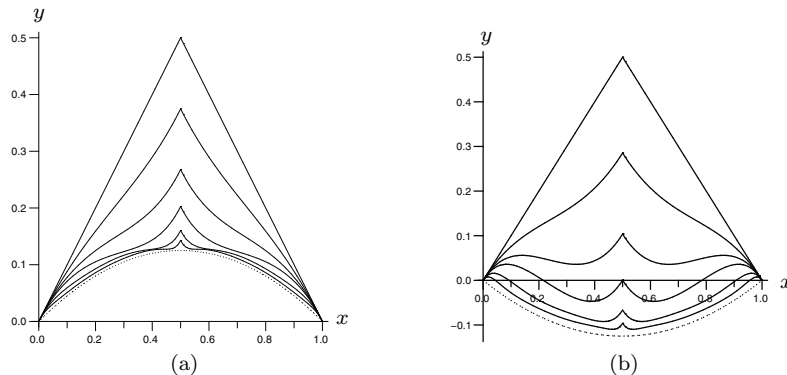


FIG. 5.6. Forward time evolution of a clamped viscida with initial profile given by (4.15) with $H_0 = 1/2$, $a = 1/2$, and (a) $P = 2$, $t = 0, 4, 10, 20, 100, 400$, (b) $P = -2$, $t = 0, 4, 10, 20, 100, 400$. In both cases the profile (5.9) is shown as a dotted line.

$x = 0$ and $H_x = -P/4$ at $x = 1$, and therefore this profile only satisfies the equation of a viscida whose ends are clamped at these specific angles. However, as for the simply supported viscida, we still find that the viscida evolves towards the steady configuration (5.9) even when the ends are not clamped at these angles, except in boundary layers where the profile satisfies the constraint (3.17), and near the corner at $x = a$.

In Figure 5.5 we apply a pressure $P = 4$, which corresponds to the special case where (5.9) satisfies the clamped-end conditions (3.17) when $H(x, 0)$ is given by (4.15) with $H_0 = 1/2$ and $a = 1/2$. Here the entire profile tends towards this configuration as $t \rightarrow \infty$.

In Figure 5.6 we consider the forward time evolution for $P = \pm 2$. As in the unpressurized case, evolution occurs more slowly when we clamp rather than simply-support the ends. When we choose $P < 0$, the profile approaches the final configuration (5.9) more slowly, since the difference between the angle at each end for the steady solution (5.9) compared to the actual clamped-end conditions (3.17) is larger in the negative-pressure case. We find that, due to the stronger constraint imposed by the clamped

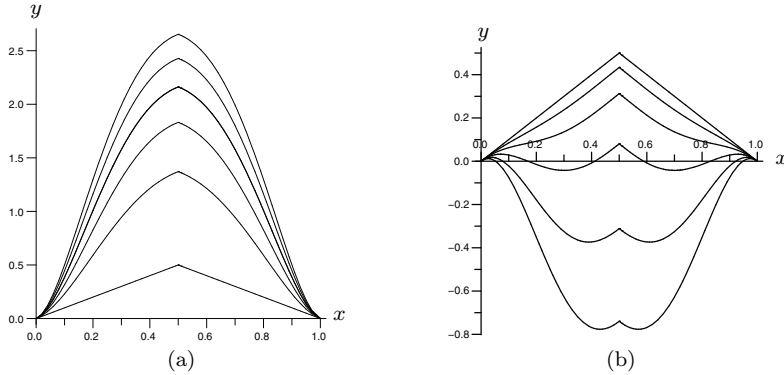


FIG. 5.7. Inverse time evolution of a clamped viscida with initial profile given by (4.15) with $H_0 = 1/2$, $a = 1/2$, and (a) $P = -100$, $t = 0, -2, -4, -6, -8, -10$, (b) $P = 10$, $t = 0, -4, -8, -12, -16, -20$.

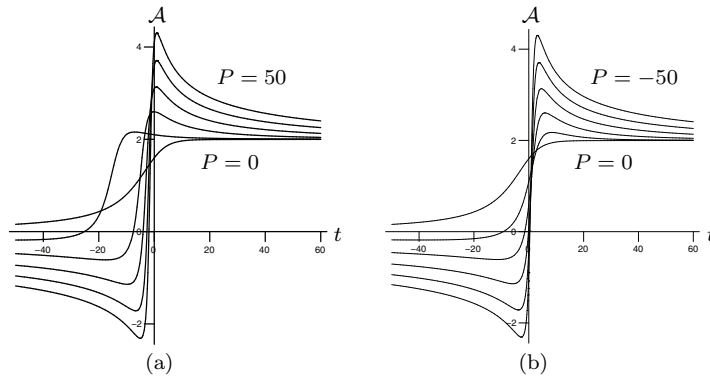


FIG. 5.8. Plot of \mathcal{A} versus t for a clamped viscida with initial profile given by (4.15) with $H_0 = 1/2$, $a = 1/2$, and (a) $P = 0, 10, 20, 30, 40, 50$, (b) $P = 0, -10, -20, -30, -40, -50$.

boundary conditions, (5.9) approximates the final viscida less effectively near the ends than in the simply supported case.

Figure 5.7(a) illustrates the inverse time evolution when $P = -100$. As for the simply supported case, we choose P to be large to produce a noticeable change from the unpressurized evolution, and again observe the profile to become more rounded with time. Applying a positive pressure in Figure 5.7(b), we observe similar behavior to the simply supported case, although, as observed for forward time, the evolution is slowed by clamping the ends.

In Figure 5.8 we plot the tension \mathcal{A} versus t for various values of applied pressure P . We find that we must choose the value of the pressure to be significantly larger than that considered for a simply supported viscida to provide comparable variations in the tension. We also find that the tension takes longer to relax towards the final positive- and negative-time values.

6. Well posedness of the inverse problem. We have demonstrated above that the viscida model (3.14) is well posed for both forward and inverse time, allowing us to determine initial profiles which would form a corner configuration at a later time. The full two-dimensional surface-tension-driven Stokes flow problem is undoubtedly ill posed when solved backwards in time, so our asymptotic simplification has had the

fortuitous side effect of eliminating unstable high-wavenumber disturbances. In this section we show how this elimination occurs by considering separable solutions of the two-dimensional Stokes equations in a viscous strip of small but finite thickness.

In terms of suitable dimensionless variables, we may consider a viscous fluid which lies between $x = 0$ and $x = 1$ with thickness ϵ but make no assumptions yet about the magnitude of ϵ . We let the free surfaces be given by

$$(6.1) \quad y = \frac{\epsilon}{2} + \alpha e^{\lambda t} \cos(n\pi x), \quad y = -\frac{\epsilon}{2} \pm \alpha e^{\lambda t} \cos(n\pi x),$$

where the positive sign corresponds to *sinuous* modes while the negative sign represents *varicose* solutions. Applying the symmetry boundary conditions at the ends

$$(6.2) \quad u = \frac{\partial v}{\partial x} = 0$$

on $x = 0, 1$, we can seek solutions of the form

$$(6.3) \quad u = F_1(y)e^{\lambda t} \sin(n\pi x), \quad v = F_2(y)e^{\lambda t} \cos(n\pi x), \quad p = F_3(y)e^{\lambda t} \cos(n\pi x).$$

The Stokes equations (2.3)–(2.5) then imply that $F_2(y)$ satisfies

$$(6.4) \quad F_2^{(4)} - 2n^2\pi^2 F_2'' + n^4\pi^4 F_2 = 0.$$

For varicose modes, the linearized versions of the kinematic and dynamic boundary conditions (2.7)–(2.9) provide

$$(6.5) \quad F_2 = \pm\lambda\alpha, \quad F_2'' + n^2\pi^2 F_2 = 0, \quad F_2^{(3)} - 3n^2\pi^2 F_2' - n^4\pi^4\alpha = 0$$

on $y = \pm\epsilon/2$, while for sinuous modes we must apply

$$(6.6) \quad F_2 = \lambda\alpha, \quad F_2'' + n^2\pi^2 F_2 = 0, \quad F_2^{(3)} - 3n^2\pi^2 F_2' \mp n^4\pi^4\alpha = 0$$

on $y = \pm\epsilon/2$.

Solving (6.4) subject to either (6.5) or (6.6) provides the respective dispersion relations for varicose and sinuous modes, namely,

$$(6.7) \quad \lambda = \lambda_v = -\frac{n\pi \sinh^2(\epsilon n\pi/2)}{\sinh(\epsilon n\pi) + \epsilon n\pi},$$

$$(6.8) \quad \lambda = \lambda_s = -\frac{n\pi \cosh^2(\epsilon n\pi/2)}{\sinh(\epsilon n\pi) - \epsilon n\pi}.$$

As $n \rightarrow \infty$ and the wavelength of the disturbances tends to zero, $\lambda \sim -n\pi/2$ for both varicose and sinuous solutions, and the problem is therefore ill posed for inverse time as expected. However, if we first take the “thin-viscida” limit $\epsilon \rightarrow 0$, we find that

$$(6.9) \quad \lambda_v \sim \frac{n^2\pi^2\epsilon}{8} + O(\epsilon^5),$$

$$(6.10) \quad \lambda_s \sim -\frac{6}{\epsilon^3 n^2 \pi^2} + O(\epsilon^{-1}),$$

so the high wavenumber sinuous modes are eliminated and the problem appears to be well posed for inverse time.

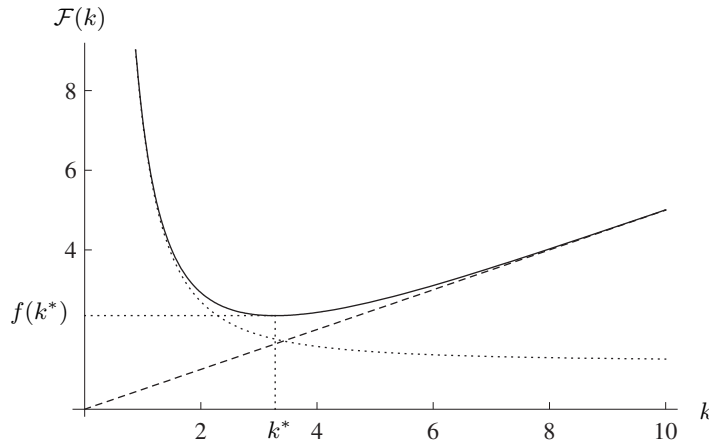


FIG. 6.1. Plot of tension $\mathcal{F}(k)$ versus k defined by (6.11). The dashed and dotted lines show the large- and small- k approximations (6.12a) and (6.12b).

Writing $k = \epsilon n\pi$ we see that

$$(6.11) \quad -\epsilon\lambda_s = \mathcal{F}(k) = \frac{k \cosh^2(k/2)}{\sinh(k) - k}$$

$$(6.12a) \quad \sim \begin{cases} \frac{k}{2} & \text{as } k \rightarrow \infty, \\ \frac{6}{k^2} + \frac{6}{5} & \text{as } k \rightarrow 0. \end{cases}$$

In Figure 6.1 we show how $\mathcal{F}(k)$ tends to infinity at both small and large wavenumbers while possessing a minimum at $k = k^* \approx 3.278$. Hence there is a critical mode $n = k^*/\epsilon\pi$ which decays most slowly at a rate $\mathcal{F}(k^*)/\epsilon$, where $\mathcal{F}(k^*) \approx 2.35$.

7. Conclusions. We considered two-dimensional Stokes flow in a fluid sheet whose ends are held a fixed distance apart, driven by surface tension and an applied pressure. We chose a domain which has a thickness much smaller than its length so that it can be modeled as a thin viscida, and furthermore, we assumed that the radius of curvature is much greater than the center-line length so that its profile is almost flat.

We derived a simplified asymptotic model, generalizing that of [1], comprising an intrinsic equation governing the evolution of the center-line of the viscida, while the viscida thickness remains constant. In the case where there is no applied pressure, we employed a change in time variable, after which we could write down the solution explicitly. The new variable is then related back to original time by an algebraic equation.

We proceeded to investigate the evolution of an initial profile containing a smoothed-off corner. We found that no adverse effects are generated by gradually increasing the curvature, and thus concluded that we can use our theory to predict the global behavior of a viscida containing localized regions of high curvature. We found that, on the timescale of interest, any corners initially present in the viscida persist for all time and are not smoothed out as we would perhaps have anticipated. For large positive time we found that an initial asymmetric profile evolves in such a way that the corner becomes symmetric, while for large negative time the entire profile assumes a symmetric configuration.

We then investigated a viscida whose ends are clamped, and found, somewhat surprisingly, that the governing equations still admit separable solutions when the ends are clamped at nonzero angles. As for the simply supported case, the viscida relaxes towards a flat sheet, though a small boundary layer near each end forms, in which the curvature becomes large, to satisfy the boundary conditions. The evolution in such regions is eventually described by the full two-dimensional Stokes equations, but any local behavior does not influence the global viscida evolution.

A pressure differential across the viscida was introduced, with the intention of investigating whether this offers any control in the evolution. The use of separable solutions in this case is problematic, and so we adopted a numerical approach. We found that in both the simply supported and clamped-end cases, application of a pressure accelerates the evolution towards the final state, which is no longer a straight line but a uniform arc. For negative time, the roles of positive and negative pressures are reversed: applying a positive pressure when time runs backwards has a qualitatively similar effect to a negative pressure when time increases.

We found that in both the simply supported and clamped-end cases, the profile relaxes towards the steady solution to the governing equations which satisfies the fixed-end constraints, except in small regions near the ends and near the corner, where the curvature is large. As in the earlier analysis, the evolution in these regions is eventually described by the full two-dimensional Stokes equations.

We note that our governing equation for the evolution of a simply supported viscida (4.7) is similar to the equation

$$(7.1) \quad \frac{\partial f}{\partial t} - \lambda \nabla^2 \frac{\partial f}{\partial t} = k \nabla^2 f,$$

where ∇^2 denotes the Laplacian operator. The initial and boundary conditions posed for (7.1) are the same as those posed for solutions of the parabolic heat equation, which is obtained by setting $\lambda = 0$. The class of equations (7.1) are called *pseudoparabolic equations* [8]. Problems which are well posed for parabolic equations are also well posed for these equations.

As well as being an intriguing canonical fluid dynamics problem in its own right, the present study was conceived as a prototype for the fabrication of glass tubing whose final cross-section contains corners. The model considered here may be thought of as a local analysis of a corner region in the two-dimensional tube cross-section. The well posedness of our model as an inverse problem allows us to identify the die shape required to produce a final tubing with corner regions. Our result regarding the preservation of the corner is also significant, as this implies that corners present in the initial die will persist and not be smoothed out during the drawing process. Our simplified model also demonstrates how a pressure differential may be used to control the shape evolution but has no influence on the corner. Ultimately, the die shape required to produce tubing with a square cross-section may be found by coupling our model for the two-dimensional evolution of the cross-section with conservation equations for axial flow along the tube as described in [4, 5].

Acknowledgments. The authors gratefully acknowledge helpful discussions with Dr. H. J. J. Gramberg, Professor E. J. Hinch, Dr. J. R. Lister, and Dr. J. R. Ockendon.

REFERENCES

- [1] J. D. BUCKMASTER, A. NACHMAN, AND L. TING, *The buckling and stretching of a viscida*, J. Fluid Mech., 69 (1975), pp. 1–20.

- [2] J. D. BUCKMASTER AND A. NACHMAN, *The buckling and stretching of a viscida II. Effects of surface tension*, Quart. J. Mech. Appl. Math., 31 (1978), pp. 157–168.
- [3] B. W. VAN DE FLIERT, P. D. HOWELL, AND J. R. OCKENDON, *Pressure-driven flow of a thin viscous sheet*, J. Fluid Mech., 292 (1995), pp. 359–376.
- [4] I. M. GRIFFITHS AND P. D. HOWELL, *The surface-tension-driven evolution of a two-dimensional annular viscous tube*, J. Fluid Mech., 593 (2007), pp. 181–208.
- [5] I. M. GRIFFITHS AND P. D. HOWELL, *Mathematical modelling of non-axisymmetric capillary tubing*, J. Fluid Mech., 605 (2008), pp. 181–206.
- [6] P. D. HOWELL, *Models for thin viscous sheets*, European J. Appl. Math., 7 (1996), pp. 321–343.
- [7] N. M. RIBE, *Bending and stretching of thin viscous sheets*, J. Fluid Mech., 433 (2001), pp. 135–160.
- [8] R. E. SHOWALTER AND T. W. TING, *Pseudoparabolic partial differential equations*, SIAM J. Math. Anal., 1 (1970), pp. 1–26.
- [9] L. J. SLATER, *Generalized Hypergeometric Functions*, Cambridge University Press, Cambridge, 1966.
- [10] J. TEICHMAN AND L. MAHADEVAN, *The viscous catenary*, J. Fluid Mech., 478 (2003), pp. 71–80.
- [11] P. WILMOTT, *The stretching of a thin viscous inclusion and the drawing of glass sheets*, Phys. Fluids, A 1 (1989), pp. 1098–1103.
- [12] C. Y. WU, A. R. D. SOMERVELL, AND T. H. BARNES, *Direct image transmission through a multi-mode square optical fiber*, Opt. Commun., 157 (1998), pp. 17–22.
- [13] C. Y. WU, A. R. D. SOMERVELL, T. G. HASKELL, AND T. H. BARNES, *Optical sine transformation and image transmission by using square optical waveguide*, Opt. Commun., 175 (2000), pp. 27–32.